Journal Name

Dalton Transactions

Pyridylpyrazole N^N Ligands Combined with Sulfonyl-Functionalised Cyclometalating Ligands for Blue-Emitting Iridium(III) Complexes and Solution-Processable PhOLEDs

Received 00th January 20xx,
Accepted 00th January 20xx

DOI: 10.1039/x0xx00000x

www.rsc.org/

Helen Benjamin,[a] Mark A. Fox,[a] Andrei S. Batsanov,[a] Hameed A. Al-Attar,[b] Chensen Li,[c] Zhongjie Ren,[c] Andrew P. Monkman,[b] and Martin R. Bryce*,[a]

A series of blue iridium(III) complexes (**12**-**15**) comprising sulfonyl-functionalised phenylpyridyl cyclometalating ligands and pyridylpyrazole N^N ligands are reported, with an X-ray crystal structure obtained for **12**. The complexes are highly emissive with photoluminescence quantum yields of 0.52 – 0.70 in dichloromethane solutions: two of the complexes (**12** and **14**) show emissions at λ_{max}^{PL} 457 nm which is considerably blue-shifted compared to the archetypal blue emitter FIrpic (λ_{max} 468 nm). The short excited state lifetimes (1.8 – 3.3 μs) and spectral profiles are consistent with phosphorescence from a mixture of ligand-centred and MLCT excited states. Density functional (DFT) and time dependent DFT (TD-DFT) calculations are in agreement with the electrochemical properties and the blue phosphorescence of the complexes. The additional mesityl substituent on the pyridylpyrazole ligand of **12** and **13** enhances the solubility of the complexes facilitating thin film formation by solution processing. Phosphorescent organic light-emitting diodes (PhOLEDs) have been fabricated using **12** or **13** in a solution-processed single-emitting layer using either poly(vinylcarbazole) (PVK) or 1,3-bis(*N*-carbazolyl)benzene (mCP) as host. The most blue-shifted electroluminescence (λ_{max}^{EL} 460 nm, $CIE_{x,y}$ 0.15, 0.21) is obtained for an OLED containing complex **12** and mCP, with a brightness of 5400 cd/m^2 at 10 V which is high for PhOLEDs with similar blue CIE coordinates using a solution-processed emitter layer.

Introduction

The varied applications of luminescent transition metal complexes[1] include biological labelling probes, ion sensors, water splitting, solar cells and emitters for phosphorescent organic light-emitting diodes (OLEDs)[2-8] and for solid-state lighting.[9,10] Cyclometalated iridium(III) complexes are especially prominent in the OLED field due to their ability to harvest both singlet and triplet excitons, which can result in internal quantum efficiencies approaching 100%.[11-13] Many complexes incorporate cyclometalated 2-phenylpyridine (ppy) ligands where the highest occupied molecular orbital (HOMO) is localised mostly on the iridium atom and the phenyl ring, and the lowest unoccupied MO (LUMO) is on the pyridyl ring. This spacial separation of HOMO and LUMO means that the emission wavelength of the complexes, which occurs from a mixture of triplet metal-to-ligand charge-transfer (^{3}MLCT) states and π–π* transitions of the ligands,[14,15] can be tuned with precision by the presence of electron-withdrawing or electron-donating substituents at specific sites on the ppy framework. Additional attractive features are that the complexes generally emit with high quantum yields and relatively short excited state lifetimes on the microsecond timescale, and they possess high photochemical and chemical stability.[11-13]

Blue emitting iridium complexes are important current targets.[16,17] Four main approaches are known to be effective in shifting the emission of iridium complexes towards the blue.[18] These are: 1) Lowering the HOMO with respect to the LUMO by introducing electron-withdrawing groups, such as fluorine[19] sulfonyl,[20] phosphoryl,[20] perfluoroalkyl,[21] perfluoroalkyl carbonyl,[22] and cyano[13] substituents at specific positions on the phenyl ring. 2) Raising the LUMO by either adding electron-donating groups such as methoxy to the pyridyl ring,[23,24] or replacing the pyridyl ring with another heterocycle with higher LUMO energy.[25]

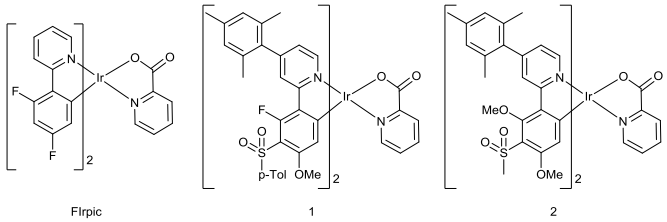

Figure 1. Previously reported picolinate complexes

[a] *Department of Chemistry, Durham University, Durham DH1 3LE, U.K. m.r.bryce@durham.ac.uk.*
[b] *Department of Physics, Durham University, Durham DH1 3LE, U.K.*
[c] *State Key Laboratory of Chemical Resource Engineering, Beijing University of Chemical Technology, Beijing 100029, China.*

Electronic Supplementary Information (ESI) available: Crystal data have been deposited with the Cambridge Crystallographic Data Base as CCDC number 1495066. Thermogravimetric data; NMR spectra; additional computational and CV data.

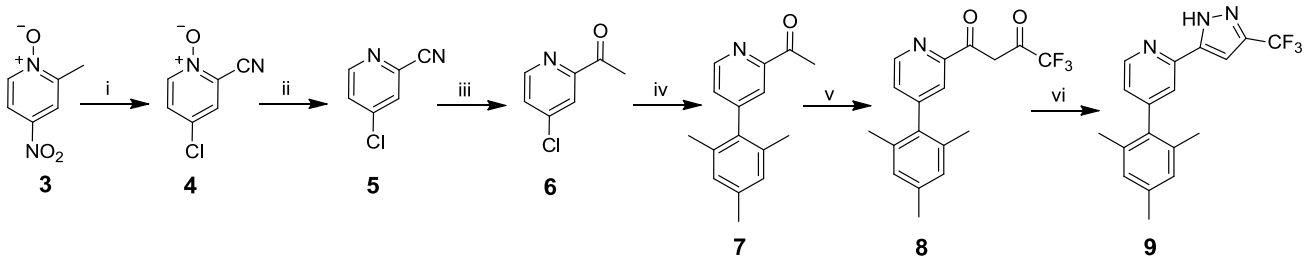

Scheme 1. Synthesis of ligand **9**. Reagents and conditions: i, CH_3COCl, 60 °C; ii, PCl_3, $CHCl_3$, reflux; iii, 1) CH_3MgCl, ether, 0 °C, 2) dilute HCl; iv, $Pd(OAc)_2$, PPh_3, 2,4,6-trimethylphenylboronic acid, Na_2CO_3, DME/water, reflux; v, KO^tBu, F_3CCO_2Et, THF, reflux; vi $N_2H_4.H_2O$, ethanol, reflux.

3) Using electron-withdrawing N^N ligands, e.g. pyridyl-azole, to modulate the electron density around the metal centre, thereby affecting the HOMO energy.[26-28] 4) Using strong σ-donor ligands, e.g. carbenes, to increase the crystal field splitting, thereby widening the HOMO-LUMO gap and shifting non-emissive d-d* metal-centred (MC) states to higher energies.[19]

The present study combines a pyridylpyrazole-based N^N ligand with sulfonyl-containing cyclometalating ligands[29] to obtain the new heteroleptic complexes **12-15** with emission blue-shifted compared to the archetypal blue emitter, FIrpic,[16] and the analogous picolinate-complexes **1** and **2**[29] (Figure 1). Pyridylpyrazole ligands blue-shift the emission due to their high acidity, reducing the electron density around the Ir centre and hence reducing the HOMO level relative to the LUMO.[30] They have also been exploited as the chromophoric ligands in *N*-heterocyclic carbene complexes[31] and in conjunction with other ligands.[32-34] The strongly electron-withdrawing CF_3 group on the pyrazole ring should further blue shift the emission.[35] The *p*-tolylsulfonyl with methylsulfonyl groups (complexes **1** and **2**) both blue shift the emission to the same extent,[29] and methoxy substituents can lead to a blue shift depending on their position on the ppy ligand.[36,37] Reducing the number of aromatic fluorine substituents, e.g. by selective replacement with methoxy, can maintain the blue colour and reduce chemical degradation of a complex during device operation.[38] Complexes **12-15** incorporate a mesityl substituent at C4 of the ppy ligand; it is known that a mesityl group at this position enhances the quantum yields of some complexes by reducing triplet-triplet quenching without affecting blue colour purity.[39-42] We also report the new mesityl substituted pyridylpyrazole ligand **9** which achieves the desired aims of increasing the solubility of the complexes **12** and **13**, in comparison with **14** and **15**, thereby facilitating film formation by solution processes without affecting the emission colour.

Synthesis and characterisation

The route to ligand **9** is shown in Scheme 1. 2-Acetyl-4-chloropyridine **6** was synthesised by reaction between 4-nitro-*α*-picoline-*N*-oxide **3** and acetyl chloride to give **4**[43] in 23% yield. An intermediate oxime has been proposed in this step.[43] The *N*-oxide was reduced using PCl_3 to produce **5**[43] in 73% yield, followed by reaction with methyl magnesium chloride to give **6** in 92% yield.[44] The mesityl group was then introduced via a Suzuki coupling of **6** with 2,4,6-trimethylphenylboronic acid to give **7** in 52% yield. The final steps, described in the literature for other analogues,[45] involved a crossed Claisen condensation reaction with ethyl trifluoroacetate to give a presumed diketone intermediate **8**, followed by a ring closing condensation reaction with hydrazine hydrate to give **9** in 20% yield.

The desired complexes **12** and **13** were then synthesised under standard conditions;[46,47] namely, reaction of the ligand **10** with $IrCl_3{\cdot}3H_2O$ and ligand **11**[29] with $[Ir(COD)Cl]_2$ in 2-ethoxyethanol to give a species presumed to be the bridged μ-dichloro diiridium dimer $[Ir(L)_2Cl]_2$. This intermediate species was then reacted *in situ* with ligand **9** to give the desired complexes **12** and **13**. The attempted synthesis of **13** using $IrCl_3{\cdot}3H_2O$ failed to yield any product and the ligand **11** could not be recovered. Difficulties in the cyclometalation of ligands containing methoxy substituents using $IrCl_3{\cdot}3H_2O$ have been reported previously.[29,36] Complexes **14** and **15** were synthesised from **10** and **11** by analogous reactions with 3-trifluoromethyl-5-(2-pyridyl)pyrazole ligand **16**.[30] Thermal gravimetric analysis (TGA) shows that all the complexes possess good thermal stability (Table S5 in SI), suggesting the complexes should be stable under device operation.

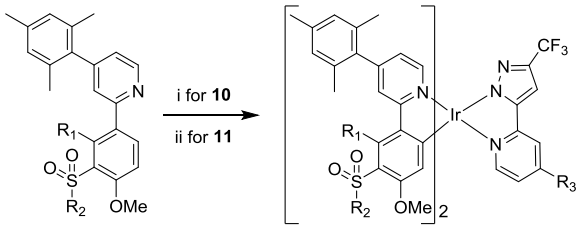

Scheme 2. Synthesis of complexes **12-15**. Reagents and conditions: i, $IrCl_3{\cdot}3H_2O$, 2-ethoxyethanol, 130 °C, followed by **9** (for **12** and **13**) or 3-trifluoromethyl-5-(2-pyridyl)pyrazole **16** (for **14** and **15**) DCM/ethanol, 55 °C; ii, $[Ir(COD)Cl]_2$, 2-ethoxyethanol, 130 °C, followed by **9** or **16**, DCM/ethanol, 55 °C.

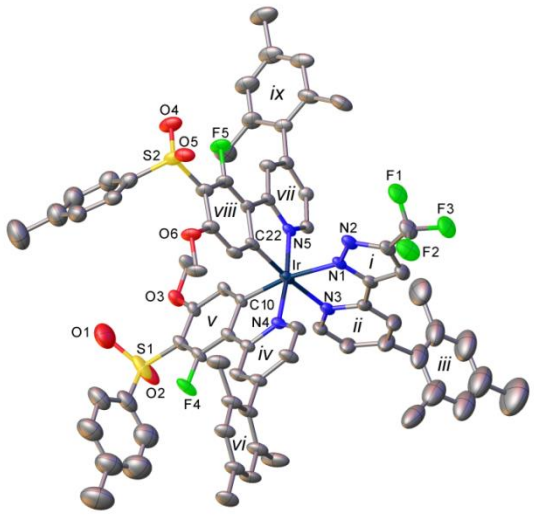

Figure 2. X-ray molecular structure of **12**. H atoms and the disorder of CF_3 group are omitted; thermal ellipsoids are drawn at the 30% probability level. Bond distances (Å): Ir–N(1) 2.102(6), Ir–N(3) 2.142(8), Ir–N(4) 2.040(6), Ir–N(5) 2.057(6), Ir–C(10) 2.006(7) and Ir–C(22) 1.991(9). Interplanar angles (°): *i/ii* 7, *ii/iii* 90, *iv/v* 7, *iv/vi* 74, *vii/viii* 4, *vii/ix* 89.

X-Ray Crystal Structure

The single crystal X-ray structure of the highly-functionalised complex **12** (Figure 2) shows a distorted octahedral coordination of the Ir atom, similar to that in its analogues.[32] The two Ir-C bonds are in *cis* positions to one another and *trans* to the Ir-N bonds of the N^N ligand, which are, therefore, elongated compared to the mutually *trans* bonds Ir-N(4) and Ir-N(5). The mesityl groups are near-perpendicular to the corresponding pyridyl rings. The crystal packing of **12** is dominated by edge-to-face contacts between arene groups, without π-π stacking.

Photophysical and Electrochemical Properties

The absorption and emission spectra of complexes **12**-**15** (Figure 3) are consistent with pyridylpyrazole subtly lowering the energy of the HOMO. All the complexes show strong absorption bands in the 250-325 nm region, assigned to the π-π* transitions on the ligands.[16,18] Absorption bands with lower extinction coefficients in the 350-450 nm range are ascribed to singlet and triplet metal-to-ligand charge-transfer (^{1}MLCT and ^{3}MLCT) states.[48,49] Here, we see differences between the picolinate complexes **1** and **2**,[29] and complexes **12**-**15**; the ^{1}MLCT bands move to higher energies on replacing the picolinate ligands with ligands **9** or **16**, suggesting the pyridylpyrazole has indeed decreased the energy of the metal d-orbitals. The emission spectra of the complexes are shown in Figure 3b. Complexes **12**-**15** emit in the blue region, and display a similar emission profile to that of FIrpic and the analogous picolinate complexes **1** and **2**. A notable feature is that the λ_{max} value for **12** and **13** is blue-shifted by 7 and 8 nm relative to their analogous picolinate complexes **1** and **2**, respectively. This represents a blue-shift of 11 nm and 2 nm relative to that of the benchmark sky-blue emitter FIrpic.[16] The impressive 11 nm shift for complex **12** is primarily a consequence of the combined benefits of the sulfone substituents and the N^N ligand. The UV-Vis absorption and emission of complexes **14** and **15** are similar to those of complexes **12** and **13**, indicating the introduction of the mesityl substituent on the N^N ligand does not impact the emission colour.

The photoluminescence quantum yield (PLQY) and lifetime data are listed in Table 1. The PLQYs for complexes **12**-**15** are comparable to their pic analogues **1** and **2**, with lifetimes and spectral profiles consistent with phosphorescence from a mixture of ligand-centred and MLCT excited states.[18,49]

The electrochemical behaviour of complexes **12**-**15** was investigated by cyclic voltammetry (CV) in a 0.1 M $N^nBu_4PF_6$ acetonitrile solution, and compared to FIrpic and picolinate analogues **1** and **2**.[29] The voltammograms of FIrpic, **12**-**15** are shown in Figures 4 and S13, and the key parameters are listed in Table 2. Whereas the picolinate complexes (FIrpic, **1** and **2**) show a single quasi-reversible oxidation wave, complexes **12**-**15** show two oxidation waves. In the case of **12** and **13** the two waves are irreversible, whereas for **14** and **15** the first oxidation wave is quasi-reversible.

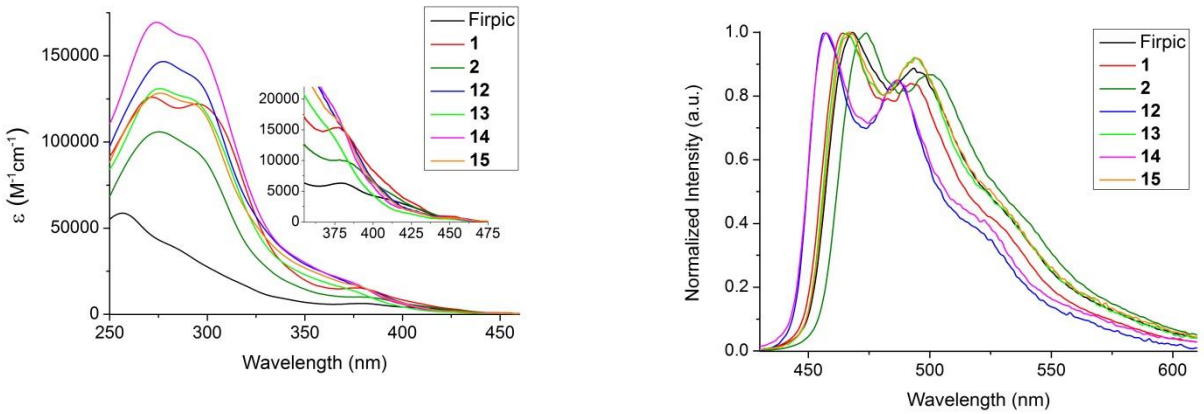

Figure 3: a) UV-Vis absorption spectra of the complexes in DCM [<10^{-5} M]. Inset shows an expansion of the 350-475 nm region. b) Emission spectra in deaerated DCM, λ_{ex} = 380 nm.

Table 1: Photophysical data for the iridium complexes.

Complex	λ_{max}^{abs} (ε)/ nm (x10^3 M^{-1} cm^{-1})[a]	λ_{max}^{em} / nm[b]	PLQY / Φ_{PL}[a,c]	τ_P / μs[a,d]	k_r / $10^5 s^{-1}$	k_{nr} / $10^5 s^{-1}$
FIrpic	277 (50.1), 301 (34.2), 304 (32.6), 337 (13.8, sh), 357 (8.9, sh), 400 (6.2), 454 (0.8)	468, 496, 531 (sh)	0.67	1.72	3.90	1.92
1[29]	258 (s sh, 108.5), 271 (128.6), 297 (123.4), 307 (sh, 112.5), 339 (s sh, 29.2), 379 (15.7), 450 (1.0)	464, 490, 524 (sh)	0.67	1.78	3.76	1.85
2[29]	275 (104.4), 291 (101.9), 324 (sh, 47.8), 381 (14.5), 405 (sh, 7.9), 456 (0.9)	474, 497, 536 (sh)	0.58	2.13	2.72	1.97
12	274 (144.4), 293 (136.7), 370 (19.4), 419 (sh,2.7), 447 (0.7)	457, 486, 521 (sh)	0.62	2.30	2.70	1.65
13	255 (sh, 100.4), 277 (125.8), 292 (133.5), 321 (59.6) (sh), 375 (16.3), 406 (sh, 5.1), 454 (0.8)	466, 494, 531 (sh)	0.52	3.13	1.66	1.53
14	274 (171.0), 291 (161), 374 (17.9), 418 (2.1), 450 (0.5)	457, 486, 522 (sh)	0.70	2.74	2.55	1.09
15	276 (129.3), 295 (122.75), 325 (50.8), 371 (18.2), 411 (3.2), 454 (0.7)	467, 494, 531 (sh)	0.64	3.30	1.94	1.09

[a] Data obtained in dichloromethane solution at 20 °C. [b] Data obtained in degassed dichloromethane solution with λ_{ex} = 380 nm. [c] Measured relative to $Ir(ppy)_3$ Φ_{PL} = 0.46 in degassed dichloromethane at 20 °C; estimated error ±5%. [d] Estimated error ±5%.

As complexes **12-15** contain a pyridylpyrazole-based ligand it is assumed the second oxidation occurs either on this ligand or is due to an interaction of this ligand with the metal. Exchanging the picolinate ancillary ligand for pyridylpyrazole results in an increase in the first oxidation potential by only 10-20 mV (**1** vs **12**, **2** vs **13**), consistent with pyridylpyrazole subtly lowering the energy of the HOMO. The presence of the mesityl group on the N^N ligand (complexes **12** and **13**) decreases the oxidation potentials by ca. 50 mV compared to the unsubstituted complexes **14** and **15**. No reduction waves were observed within the solvent window to -2.0 V. This is consistent with the calculated large HOMO-LUMO gap (Table 2).

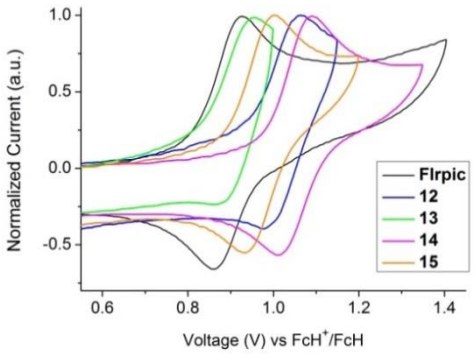

Figure 4: Cyclic voltammograms of the iridium complexes.

Computations

Electronic structure calculations were carried out on the four new iridium complexes **12-15** to explore the frontier orbitals (Figure 5 and Tables S1-S4) in order to support the electrochemical and photophysical observations. The full geometries were optimised at B3LYP/LANL2DZ:3-21G* to compare directly with computed data of FIrpic, **1** and **2** reported earlier.[29] The optimised geometries are denoted as **12'-15'** to identify them as computed models and distinguish the predicted data from experimental data. Comparison between optimised (**12'**) and X-ray determined (**12**) geometry reveals good agreement with differences in bond lengths below 0.04 Å.

Complexes **12'-15'** have HOMOs similar to FIrpic with the HOMO on iridium and phenyl (ppy) (Figure 5). The lower HOMO energies on the complexes **12'-15'**, compared to FIrpic, reflect the electron-withdrawing properties of the sulfone groups. Frontier orbital energies for all complexes are listed in Table 2 for direct comparison with the observed CV data. The trends in observed and computed HOMO energies are in very good agreement. The iridium contributions (32-33%, Table 3) in the HOMOs of **12'-15'** are lower than the corresponding contribution in FIrpic' (44%) suggesting increased ligand contributions in the MLCT transitions involved in the emissions of **12'-15'** with respect to MLCT transitions for FIrpic'.

The LUMOs in **12'-15'** have substantial contributions from the pyridyl groups of the ppy and the pyridylpyrazole ligands which raise their orbital energies compared to FIrpic' where the LUMO is entirely located on the pyridyl group of the ppy ligands. The pyridylpyrazole ligands are, therefore, not ancillary. Consequently, the HOMO-LUMO energy gaps (HLGs) in complexes **12'-15'** are larger than the HLG in FIrpic' (Table 2) which is consistent with the observed blue-shifted emissions of **12-15** compared to FIrpic. The LUMOs in **13'** and **15'** contain more pyridylpyrazole character than ppy character (Figure 5) which is explained by the increased number of electron-donating methoxy groups present in the ppy ligands of these complexes.

Table 2: Cyclic voltammetric data of the iridium complexes.

Complex	$E^{ox1}_{1/2}$ / V[a]	$E^{ox2}_{1/2}$ / V[a]	Obs *E*(HOMO) / V[c]	Complex	Calc HOMO / eV	Calc LUMO / eV	Calc HLG / eV[d]
FIrpic[29]	0.89	-	-5.69	FIrpic'	-5.49	-1.87	3.62
1[29]	1.01	-	-5.81	**1'**	-5.64	-1.94	3.70
2[29]	0.89	-	-5.69	**2'**	-5.53	-1.89	3.64
12	1.02[b]	1.28[b]	-5.82	**12'**	-5.74	-1.83	3.91
13	0.91[b]	1.17[b]	-5.71	**13'**	-5.62	-1.77	3.85
14	1.07	1.41[b]	-5.87	**14'**	-5.77	-1.89	3.88
15	0.97	1.28[b]	-5.77	**15'**	-5.64	-1.84	3.80

[a] Redox data were obtained in 0.1 M NBu_4PF_6 acetonitrile solutions and are reported vs. FcH/FcH^+.[50] [b] Not reversible. [c] E(HOMO) = –4.8 – $E^{ox1}_{1/2}$ with respect to the FcH/FcH^+ couple at 4.8 V. [d] HLG = HOMO-LUMO energy gap.

TD-DFT computations were carried out on the S_0 optimised geometries of **12'-15'** to predict emission wavelengths of these complexes. The initial excitation is assumed to give the lowest energy singlet excited state S_1 which in the presence of the iridium centre results in intersystem crossing (ISC) to form the triplet excited state T_1 and phosphorescence is observed from the $S_0 \leftarrow T_1$ process. The small Stokes shifts observed for these complexes suggest that the T_1 geometry is similar to the corresponding S_0 geometry. The reverse process $S_0 \leftarrow T_1$ is thus considered to have the same nature as the computed $S_0 \rightarrow T_1$ process with the predicted emission wavelength adjusted to take into account the Stokes shift. Table 3 shows there is close agreement between the predicted $S_0 \leftarrow T_1$ wavelengths and the observed emission wavelengths for all the complexes.

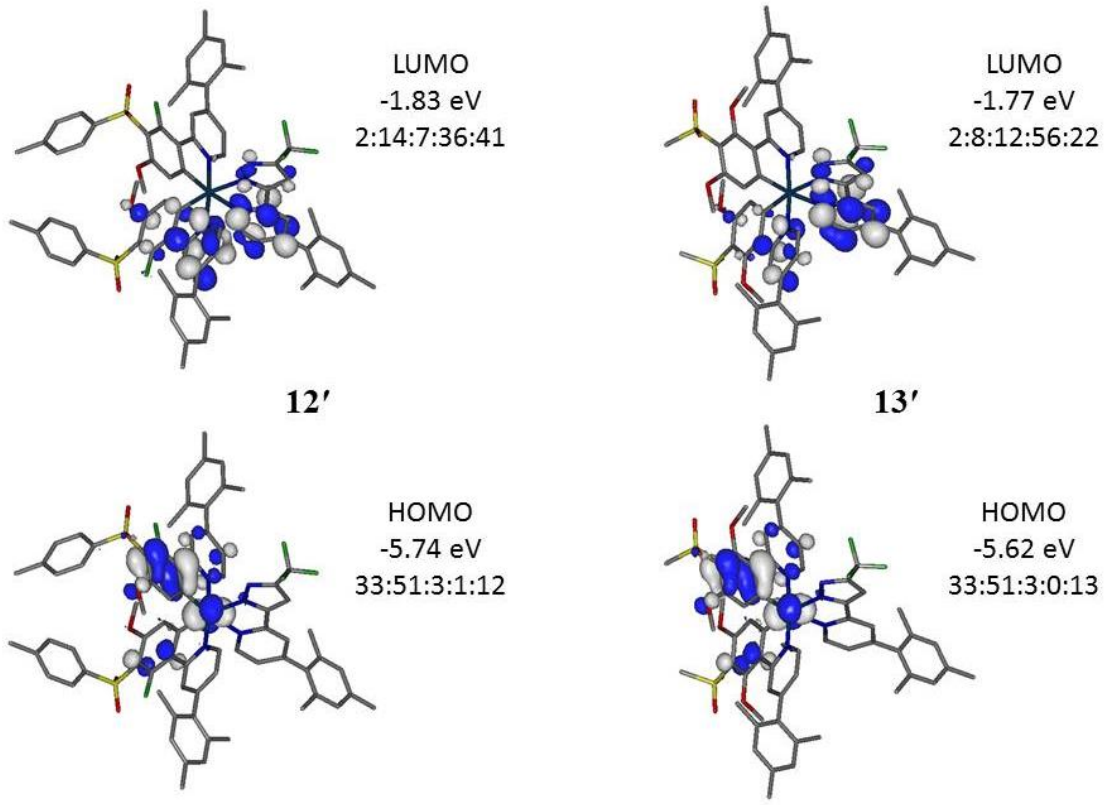

Figure 5. Frontier molecular orbitals for **12′** and **13′**. All contours are plotted at ±0.04 (e/bohr^3)$^{1/2}$. Ir : phenyl : pyrazolyl : pyridyl(pypz): pyridyl(ppy) % orbital contribution ratio are listed for each orbital.

Table 3. Iridium atom contributions in HOMOs and predicted (TD-DFT) emission wavelengths of iridium complexes

Complex	% Ir HOMO	$S_0 \leftarrow T_1$ nm [a]	Complex	Observed λ_{max}^{em} / nm [b]
FIrpic′[29]	44	471	FIrpic	471
1′[29]	39	467	**1**	464
2′[29]	40	473	**2**	474
12′	33	455	**12**	457
13′	33	459	**13**	466
14′	32	454	**14**	457
15′	32	459	**15**	467

[a] Values from TD-DFT data on S_0 optimised geometries with scaling energy factor of 0.945 based on dichloromethane at 298 K. [b] Observed highest energy band from emission spectra (Table 1).

Phosphorescent Organic Light-emitting Devices

PhOLEDs containing complex **12**, **13** or **2** as the dopant complex were fabricated to compare directly with our reference devices containing FIrpic and **1**. The initial standard device architecture comprised of a simple single-emissive-layer which was a blend of poly(vinylcarbazole) (PVK) as the host material, OXD-7 (an electron-transporting material) and the Ir complex to give the architecture: ITO/PEDOT:PSS (45 nm)/PVK:OXD-7(30wt%):Ir complex(15wt%) (60 nm)/TPBi (30 nm)/LiF (1 nm)/Al (100 nm). The emissive layer was spin-coated from chlorobenzene solution to prevent possible degradation of the complexes which is known to occur during thermal evaporation of complexes which have fluorinated ligands.[38,51-54] TPBi was used as an additional electron transporting layer adjacent to the cathode to improve charge balance and to ensure that excitons are confined in the emitter layer.[55] The efficiency and luminance data of the devices are summarised in Table 4 and the electroluminescence (EL) spectra are shown in Figure 6a. The EL and PL spectra are similar for all the complexes due to efficient exciton confinement on the emissive molecules. The λ_{max}^{EL} of complex **12** is significantly bluer (by 6 nm) than the corresponding pic complex **1**. However, as a trade-off, **12** has lower brightness (panel e), lower EQE (panel c), and lower current and power efficiencies (panels d and f). Based on the electrochemical data, the HOMO of **12** is lower in energy than **1**, which could be partially responsible for the reduced performance. Complex **13**, however, performed better than **2**, with comparable brightness and turn-on voltage (panel e), and with superior EQE, current and power efficiencies. The λ_{max}^{EL} of **13** is also blue-shifted relative to **2**; however, this is offset by a broader emission resulting in similar CIE coordinates for both complexes. The additional mesityl substituent on the N^N ligand of **12** and **13** enhances the solubility of the complexes facilitating thin film formation by solution processing.

We further explored the bluest complex **12** using mCP as a wide energy gap host which is more appropriate for a deep blue emitter in the architecture: ITO/TAPC (45 nm)/mCP:Ir complex **12**(15wt%) (45 nm)/Tm3PyBP (5 nm)/TPBi (30 nm)/LiF (1 nm)/Al (100 nm). TAPC served as a hole-transporting layer and Tm3PyBP serves as an additional hole/exciton-blocking layer to optimise the device structure.[56] Compared to the **12**:PVK device, the **12**:mCP device displayed a significantly lower turn-on voltage and further blue shifted electroluminescence to λ_{max}^{EL} 460 nm, $CIE_{x,y}$ (0.15, 0.21) with an increased maximum EQE of 6.3% and increased brightness at 10 V of 5400 cd/m^2 which is high compared to reported PhOLEDs with similar blue CIE coordinates using a solution-processed emitter layer.[57]

Conclusions

To summarise, replacing the picolinate ancillary ligand of the heteroleptic iridium complexes **1** and **2** with a pyridylpyrazole-based ligand affords the new complexes **12-15** with blue shifted emission. This is ascribed to a reduction of electron density around the metal centre which results in a lowering of the energy of the HOMO of the complexes, as observed in the solution electrochemical data. (TD-)DFT calculations are in excellent agreement with the observed photophysical and electrochemical properties of the complexes. Blue-emitting PhOLEDs have been fabricated with a solution-processed emissive layer structure. Notably, devices of complex **12** possess λ_{max}^{EL} 460 nm and $CIE_{x,y}$ (0.15, 0.21) with brightness at 10 V of 5400 cd/m^2. This study demonstrates that the rational design of new complexes with specific functionalities on the cyclometalating and the N^N ligands is an effective route to new efficient blue emitters and PhOLEDs using relatively simple device architectures.

Table 4. Summary of device data

Complex	λ_{ELmax} / nm	Brightness (max, and at 10 V) / cd/m^2	turn-on voltage / V [c]	EQE_{max} / %	current efficiency / cd/A	power efficiency / lm/W	CIE coordinates / (x,y) [d]
FIrpic [a]	475	7340, 2380	6.2	5.4	12.2	5.1	(0.19, 0.38)
1 [a]	470	2072, 175	8.5	3.5	6.1	1.9	(0.16, 0.30)
2 [a]	478	516, 160	8.5	1.2	2.6	0.9	(0.22, 0.40)
12 [a]	464	1066, 55	9.5	2.3	4.1	1.2	(0.17, 0.28)
13 [a]	473	456, 195	7.9	1.7	3.9	1.4	(0.23, 0.40)
12 [b]	460	5428, 5400	6.2	6.3	6.9	3.5	(0.15, 0.21)

[a] In PVK host. [b] In mCP host. [c] Measured at a brightness of 10 cd/m^2. [d] Measured at 12 V.

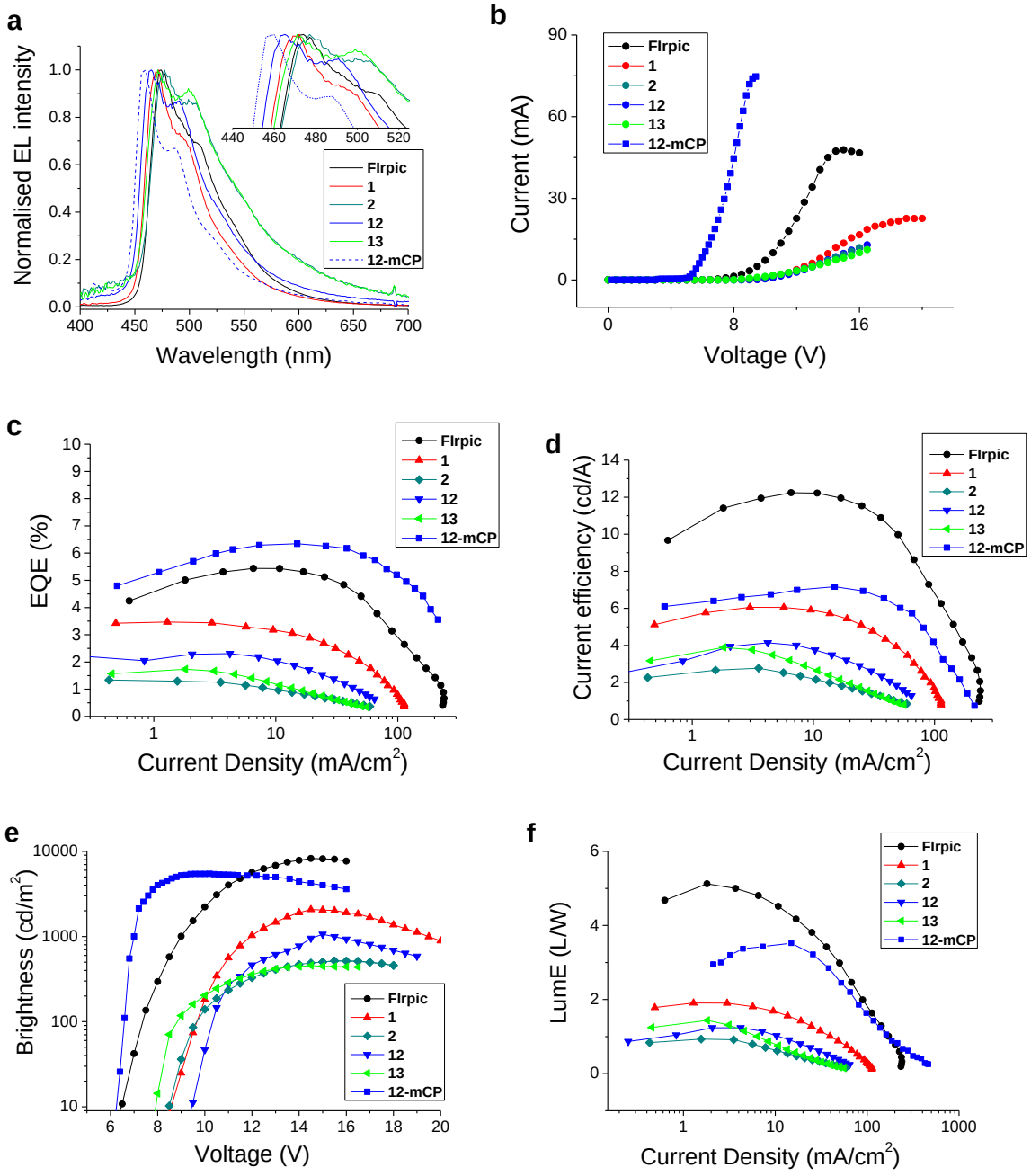

Figure 6: Electroluminescent device data for complexes FIrpic, **1**, **2**, **12** and **13** in PVK host and for **12** in mCP host.

Experimental Section

Materials, Synthesis and Characterization. All commercially available chemicals were used without further purification. Reactions requiring an inert atmosphere were performed under a blanket of argon gas, which was dried over a phosphorus pentoxide column. Anhydrous solvents were dried through an HPLC column on an Innovative Technology Inc. solvent purification system. Column chromatography was performed using 40-60 µm mesh silica gel. Analytical TLC was performed on plates pre-coated with silica gel (Merck, silica gel 60F254) and visualised using UV light (254, 315, 365 nm). NMR spectra were recorded on a Bruker Avance 400 MHz spectrometer. Chemical shifts are referenced to tetramethylsilane [TMS, $Si(CH_3)_4$] at 0.00 ppm. Melting points were determined in open-ended capillaries using a Stuart Scientific SMP3 melting point apparatus at a ramping rate of 1 ^{o}C/min and were recorded to the nearest 0.1 ^{o}C. ESI and MALDI mass spectra were recorded on a Thermo-Finnigan LTQ FT (7.0 T magnet) spectrometer. ASAP mass spectra were recorded on a Waters Xevo QTOF spectrometer. GCMS spectra were recorded on a Thermo-Finnigan Trace GCMS (EI and CI ion sources). Elemental analyses were obtained on an Exeter Analytical Inc. CE-440 elemental analyzer.

Solution electrochemistry and photophysics. Cyclic voltammetry experiments were recorded using a BAS CV50W electrochemical analyzer fitted with a three-electrode system consisting of a Pt disk (Ø = 1.8 mm) as the working electrode, a Pt wire as an auxiliary electrode and an $Ag/AgNO_3$ (0.1 M $[NEt_4][ClO_4]$ in CH_3CN) system as the reference electrode. Experiments were conducted in dry acetonitrile solution with $N^nBu_4PF_6$ (0.1 M) as the supporting electrolyte at a scan rate of 100 mV/s. The reference electrode was assumed to be stable and was referenced externally to ferrocene (Cp_2Fe) and decamethylferrocene (Cp^*_2Fe) which displayed potentials ($E_{1/2}$) of -0.41 V and +0.10 V, respectively, versus $Ag/AgNO_3$ under these conditions. It was not possible to use Cp_2Fe or Cp^*_2Fe as an internal reference because their addition to the solutions of the complexes resulted in a distortion of the redox waves of the complexes.

Solution state photophysical data were obtained using freshly prepared solutions of the complexes in DCM. Emission and lifetime measurements used thoroughly degassed solutions achieved by three freeze-pump-thaw cycles, and quartz cuvettes with a path length of 1 cm. The solutions had absorbance below 0.10 to minimise inner filter effects. UV-vis absorption measurements were recorded using a Unicam UV2-100 spectrometer operated with Unicam Vision(ver. 3.50) software. Baseline correction was achieved by reference to pure solvent in the same cuvette. Absorption measurements were obtained using quartz cuvettes with a path length of 2 cm. Excitation and emission spectra were recorded on a Jobin-Yvon-Horiba SpexFluoromax 3 Spectrometer. Solutions of the complexes in degassed DCM [$<10^{-5}$ M] were used for decay measurements. Samples were excited with a pulsed Nitrogen laser emitting at 337.1 nm. Emission was focused onto a spectrograph and detected on a sensitive gated iCCD camera (Stanford Computer Optics) with sub-nanosecond resolution. Solution PLQYs were recorded in degassed solvent, and determined using the relative method, with $Ir(ppy)_3$ (Φ_{PL} = 0.46 in degassed dichloromethane, determined in-house vs Φ_{PL} = 0.546 in 0.5 M H_2SO_4) as the reference. The PLQYs were calculated according to the following equation:

$$\Phi_x = \Phi_{ref}\frac{Grad_x}{Grad_{ref}}.\left(\frac{\eta_x}{\eta_{ref}}\right)^2$$

where subscripts 'x' and 'ref' denote the material being measured and the reference, respectively. Φ represents the PLQY, Grad is the gradient from the plot of integrated fluorescence intensity vs absorbance, and η is the refractive index of the solvent.

Thermal Analyses. Thermogravimetric analysis (TGA) was performed in a nitrogen atmosphere using a Perkin-Elmer Pyris 1 TGA instrument. The complexes were heated at a rate of 10 ^oC /min from room temperature up to 600 ^oC.

Computational studies. All calculations were carried out with the Gaussian 09 package.[58] All optimised S_0 geometries for **12'**-**15'** were carried out using B3LYP[59]with the pseudopotential (LANL2DZ)[60] for iridium and 3-21G* basis set for all other atoms.[61] This model chemistry was selected for direct comparison with computed data on FIrpic', **1'** and **2'**.[29] Electronic structure and TD-DFT calculations were also from the optimised geometries at B3LYP/LANL2DZ:3-21G*. The MO diagrams and orbital contributions were generated with the aid of Gabedit[62] and GaussSum[63] packages, respectively.

Phosphorescent Organic Light-emitting Devices (PhOLEDs). PhOLEDs with poly(vinylcarbazole) (PVK) host were fabricated on indium tin oxide (ITO)-coated glass substrates of thickness 125 nm and possessing a sheet resistance of 15 Ω/square. Poly(3,4-ethylenedioxythiophene) doped with high work function hole injection layer poly(styrenesulfonic acid) (PEDOT:PSS) (HIL1.3) from CLEVIOS was spin-coated at 2500 rpm for 60 s to produce a ~50 nm thick hole-injecting/transporting layer (HTL). The PEDOT:PSS layer was annealed at ca. 200 ^oC for 5 min to remove any residual water. A chlorobenzene solution of 25 mg/ml of poly(vinylcarbazole) (PVK) (Mw=90000) was doped with 30% w/w of (1,3-phenylene)bis[5-(4-*tert*-butylphenyl)-1,3,4-oxadiazole] (OXD-7). Blended devices were made by mixing 15% w/w of the Ir complexes. The prepared mixtures were filtered with a 0.45 μm pore filter and spin-coated at 2500 rpm for 1 min on the top of the PEDOT:PSS layer and baked for 10 min at 120 ^oC. Each sample was shadow masked to produce four identical devices of area 4 x 5 mm; the samples were then introduced into a nitrogen glove box, where 30 nm of 2,2',2''-(1,3,5-benzenetriyl)tris-[1-phenyl-1*H*-benzimidazole] (TPBi) was evaporated as an electron injection /hole blocking layer at a rate of ~1 A/s under vacuum at a pressure of ca. 1 x 10^{-6} torr, followed by 0.8 nm LiF and a 100 nm capping layer of aluminium under the same evaporation conditions. Therefore, the device configuration for all complexes was: ITO/PEDOT:PSS (50 nm)/PVK:OXD-7 (35%):Ir-Complex (15%)/TPBi (30 nm)/LiF(0.8 nm)/Al(100 nm). All samples were encapsulated inside a glove box using DELO UV cured epoxy (KATIOBOND) and capped with a 1.2 x 1.2 cm microscope glass slide then exposed to UV light for 3 min. Current-voltage data, device efficiency, brightness and electroluminescence spectra were measured in a calibrated Labsphere LMS-100 integrating sphere. A home written NI LabVIEW programme was used to control an Agilent 6632B DC power supply, and the emission properties of the device were measured using an Ocean Optics USB4000 CCD fibre optic spectrometer. The thicknesses of the various layers in the device were measured with a J A Woolam VASE Ellipsometer using thin films which had been spin-coated on Si/SiO_2 substrates under the same conditions as the device films.

Devices with 1,3-bis(*N*-carbazolyl)benzene (mCP) host were fabricated as follows. TAPC (1,1-bis{4-*N,N*-di(*p*-tolyl)amino]phenyl}cyclohexane), TPBi, and Tm3PyPB (1,3,5-tris(3-pyridyl-3-phenyl)benzene) were obtained from commercial sources. Indium tin oxide (ITO)-coated glass with a sheet resistance of 10 Ω per square was used as the substrate. Before device fabrication, the ITO-coated glass substrate was precleaned and exposed to UV-ozone for 15 min. PEDOT:PSS was then spin-coated onto the clean ITO substrate as a hole-injection layer. Next a mixture of complex **12** and mCP in chlorobenzene was spin-coated (10 mg/mL; 3000 rpm) to form

a ca. 45 nm thick emissive layer and annealed at 80 °C for 30 min to remove the residual solvent. Finally, a 5 nm-thick hole/exciton blocking layer of Tm3PyPB was vacuum deposited followed by a 30 nm-thick electron-transporting layer (ETL) of TPBi, and a cathode composed of a 1 nm-thick layer of LiF and aluminum (100 nm) was sequentially deposited through shadow masking at a pressure of 10^{-6} Torr. The OLED devices had a pixel sise of 4 mm × 4 mm. All measurements were performed at room temperature under ambient conditions.

Synthesis of ligands and complexes

1-(4-Mesitylpyridin-2-yl)ethanone 7

2-Acetyl-4-chloropyridine **6**[44] (1.5 g, 9.68 mmol), 2,4,6-trimethylphenylboronic acid (1.75 g, 10.67 mmol) and PPh_3 (657 mg, 2.50 mmol) were dissolved in DME (70 mL) and the solution was degassed for 20 min by bubbling with argon. Separately, an aqueous solution of Na_2CO_3 (4.18 g, 39.43 mmol in 17 mL) was degassed. The solutions were combined and $Pd(OAc)_2$ (130 mg, 0.58 mmol) was added. The mixture was heated to reflux overnight under an atmosphere of argon. The solution was then cooled to RT, and the majority of the solvent was removed *in vacuo*. DCM and water were added, and the organic layer separated. The aqueous layer was extracted with additional DCM, and the extracts combined and the solvent removed *in vacuo*. The crude residue was purified by column chromatography (DCM), followed by recrystallization from hexane to give 1-(4-mesitylpyridin-2-yl)ethanone **7** (1.2 g, 52%); m.pt. 118.9-119.9 °C; δ_H (400 MHz; $CDCl_3$) 8.74 (1H, dd, *J* 4.9, 0.8), 7.88 (1H, dd, *J* 1.7, 0.8), 7.31 (1H, dd, *J* 4.9, 1.7), 6.95 –6.94 (2H, m), 2.79 (3H, s), 2.33 (3H, s), 1.97 (6H, s); δ_C (101 MHz; $CDCl_3$) 200.07, 153.73, 151.14, 149.18, 138.05, 135.64, 135.08, 128.61, 128.41, 123.06, 26.19, 21.19, 20.72; HRMS (FTMS+ESI): calcd for $[C_{16}H_{17}NO+H]^+$: 240.1388. Found: 240.1388.

4-Mesityl-2-(3-(trifluoromethyl)-1*H*-pyrazol-5-yl)pyridine 9

A solution of 4-mesityl-2-acetylpyridine **7** (1.20 g, 5.01 mmol) in THF (15 mL) was added dropwise to a stirred suspension of KO^tBu (0.68 g, 6.06 mmol) in dry THF solution (30 mL) which was cooled in an ice bath. After 5 min ethyl trifluoroacetate (0.65 mL, 5.51 mmol) was added slowly. The solution was allowed to stir at 0 °C for 15 min before being removed from the ice bath. The mixture was heated to reflux overnight before being cooled, and the solvent was removed under reduced pressure. Water (30 mL) was added to the resulting solid to form a suspension which was neutralised with conc. HCl. The solution was then extracted with DCM. The organic phase was dried over $MgSO_4$ and the solvent removed to give the presumed 1,3-dione intermediate **8** (not characterised). This was dissolved in ethanol (30 mL) and hydrazine hydrate (0.34 mL, 95%) was added. The solution was heated to reflux overnight before the solvent was removed *in vacuo*. The residue was dissolved in DCM and washed with water to remove unreacted hydrazine hydrate. The solvent was removed, and the oily residue was redissolved in ethanol and conc. HCl (0.5 mL) was added (to promote complete dehydration). The solution was heated to reflux for 5 h, before being cooled and the solvent removed. The crude solid was dissolved in DCM and washed with water, before being dried over $MgSO_4$ and concentrated *in vacuo*. The crude solid was purified by column chromatography (1:3 EtOAc:DCM v/v) followed by recrystallization from hexane to give an off-white solid, 4-mesityl-2-(3-(trifluoromethyl)-1*H*-pyrazol-5-yl)pyridine **9** (277 mg, 20%); m.pt. 171.1-172.9 °C; δ_H (400 MHz; $CDCl_3$) 11.95 (1H, br s), 8.70 (1H, dd, *J* 5.0, 0.9), 7.47 (1H, dd, *J* 1.5, 0.9), 7.15 (1H, dd, *J* 5.0, 1.5), 6.96-7.00 (2H, m), 6.91 (1H, s), 2.35 (3H, s), 2.02 (6H, s); δ_F (376 MHz; $CDCl_3$) -62.34 (3F, s); δ_C (101 MHz; $CDCl_3$) 151.57, 149.86, 146.91, 144.42 (q, *J* 38.4), 143.10, 138.08, 135.43, 134.97, 128.52, 125.07, 121.40, 121.14 (q, *J* 267.9), 101.34, 21.06, 20.57; HRMS (FTMS+ESI): calcd for $[C_{18}H_{16}N_3F_3+H]^+$: 332.1375. Found: 332.1379.

Iridium complex 12

$IrCl_3.3H_2O$ (66 mg, 0.19 mmol) was added to a stirred solution of 2-(2-fluoro-4-methoxy-3-tosylphenyl)-4-mesitylpyridine **10**[29] (169 mg, 0.38 mmol) in 2-ethoxyethanol (5 mL). The solution was heated to 130 °C under an argon atmosphere overnight, during which time a bright yellow precipitate formed, presumed to be the dichloro bridged dimer. The solvent was removed *in vacuo* and the precipitate was redissolved in DCM/ethanol (20 mL, 3:1 v/v). 4-mesityl-2-(3-(trifluoromethyl)-1*H*-pyrazol-5-yl)pyridine **9** (77 mg, 0.28 mmol) was added and the solution was heated at 60 °C overnight under an argon atmosphere. The solution was cooled and the solvent was removed *in vacuo*. The residue was purified by column chromatography (EtOAc in DCM, 2.5% increased to 4%) to give a yellow solid, iridium complex **12** (190 mg, 70%); Anal. Calc. for $C_{74}H_{65}F_5IrN_5O_6S_2$: C, 60.39; H, 4.45; N, 4.76. Found: C, 60.53; H, 4.71; N, 4.50; δ_H (400 MHz; $CDCl_3$) 8.12-8.17 (1H, m), 8.03-8.08 (1H, m), 7.89 (2H, d, *J* 8.2), 7.88 (2H, d, *J* 8.2), 7.67 (1H, d, *J* 5.9), 7.64 (1H, d, *J* 5.9), 7.59 (1H, dd, *J* 1.7, 0.8), 7.57 (1H, d, *J* 5.9), 7.27 (4H, t, *J* 8.7 Hz), 7.02 – 6.89 (8H, s), 6.78 (2H, td, *J* 6.1, 1.8), 5.79 (1H, s), 5.74 (1H, s), 3.47 (3H, s), 3.44 (3H,s) 2.39 (3H, s), 2.38 (3H, s), 2.34 (3H, s), 2.33 (6H, s), 2.09 (3H, s), 2.01 (3H, s), 1.98 (3H, s), 1.97 (3H, s), 1.86 (6H, s); δ_F (376 MHz; $CDCl_3$) -59.87 (3F, s), -110.50 (1F, s), -111.36 (1F, s); HRMS (FTMS+ESI): calcd for $[C_{74}H_{65}N_5F_5O_6S_2{}^{191}Ir+H]^+$: 1470.3981. Found: 1470.3995. Single crystals of **12**·$3CH_2Cl_2$ for X-ray study were grown by layering of hexane over a DCM solution of **12**; they instantly decomposed when taken out of the solvent. The X-ray experiment was carried out at *T*=120 K on a D8 Venture (Bruker AXS) 3-circle diffractometer equipped with a IμS Mo microsource (Mo-*K*α radiation, focussing mirrors, $\bar{\lambda}$=0.71073 Å) and a PHOTON 100 CMOS area detector. The structure was solved by direct methods (SHELXS v. 2013/1 program[64]) and refined by full-matrix least squares using SHELXL v. 2014/7[65] and OLEX2[66] software. *Crystal data*: $C_{74}H_{67}F_5IrN_5O_6S_2 \cdot 3CH_2Cl_2$, *M*=1726.40, triclinic, space group *P*-1 (no. 2), *a*= 14.209(1), *b*= 18.215(1), *c*= 18.780(1) Å, α= 67.984(2), β= 86.202(2), γ= 69.653(2)°, *V*= 4213.6(5) Å^3, *Z*=2, D_c=1.361 g cm^{-3}, μ=1.89 mm^{-1}, 57359 reflections with 2θ≤50°, 14940 unique, R_{int}=0.048, *R*=0.069 [11521 data with $I \geq 2\sigma(I)$], w$R(F^2)$=0.201 (all data). CCDC-1495066. The structure contains DCM of crystallization, of which 1.5 molecules per asymmetric unit were located and the rest (presumably disordered along infinite channels parallel to the *x* axis) was masked using PLATON SQUEEZE program.[67,68] The large atomic displacement parameters,

together with practical absence of Bragg diffraction at 2θ>50°, indicate severe internal strain, probably caused by partial solvent loss.

Iridium complex 13

$[Ir(COD)Cl]_2$ (90 mg, 0.13 mmol) was added to a stirred solution of 2-(2,4-dimethoxy-3-(methylsulfonyl)phenyl)-4-mesitylpyridine **11**[29] (226 mg, 0.55 mmol) in 2-ethoxyethanol (5 mL). The solution was heated to 130 °C under an argon atmosphere overnight before being cooled to RT. Water was added and a yellow precipitate formed which was filtered, washed with more water and dried. The precipitate, presumed to be the intermediate dichloro bridged dimer, was dissolved in DCM/ethanol (40 mL, 3:1 v/v) and 4-mesityl-2-(3-(trifluoromethyl)-1*H*-pyrazol-5-yl)pyridine **9** (90 mg, 0.27 mmol) was added and the solution was heated at 55 °C overnight under an argon atmosphere. The solution was cooled and the solvent was removed *in vacuo*. The residue was purified by column chromatography (EtOAc in DCM: gradient elution from 0% to 15%) to give a yellow solid, iridium complex **13** (98 mg, 27%); Anal. Calc. for $C_{64}H_{63}F_3IrN_5O_8S_2$: C, 57.21; H, 4.73; N, 5.21. Found: C, 57.17; H, 5.07; N, 4.68; δ_H (400 MHz; CD_2Cl_2) 8.47 (1H, d, *J* 1.4), 8.38 (1H, d, *J* 1.4), 7.80 – 7.74 (3H, m), 7.65 (1H, dd, *J* 1.8, 0.8), 6.98 (5H, s), 6.95 (2H, s), 6.91 (1H, dd, *J* 5.7, 1.8), 6.84 (1H, dd, *J* 5.9, 1.9), 6.81 (1H, dd, *J* 5.9, 1.9), 6.03 (1H, s), 6.01 (1H, s), 3.88 (3H, s), 3.85 (3H, s), 3.61 (3H, s), 3.60 (3H, s), 3.22 (3H, s), 3.19 (3H, s), 2.33 (3H, s), 2.32 (3H, s), 2.31 (3H, s), 2.09 (3H, s), 2.06 (3H, s), 2.05 (3H, s), 2.01 (3H, s), 1.88 (3H, s), 1.85 (3H, s); δ_F (376 MHz; $CDCl_3$) -58.48 (s); HRMS (FTMS+ESI): calcd for $[C_{64}H_{63}F_3N_5O_8S_2{}^{191}Ir+H]^+$: 1342.3754. Found: 1342.3802.

2-(3-(Trifluoromethyl)-1*H*-pyrazol-5-yl)pyridine 16

2-Acetylpyridine (1.00 g, 8.25 mmol) and ethyltrifluoroacetate (2.35 g, 16.51 mmol) were added dropwise simultaneously to a stirred suspension of NaH (396 mg, 16.51 mmol) in THF (20 mL, dry) with caution (gas evolution). The mixture was stirred at RT for 30 min before being heated to reflux overnight. The reaction was cooled and quenched with water. The reaction mixture was acidified to pH 6 with dilute HCl (2 M) and then extracted with EtOAc (3 x 60 mL). The organic phases were combined, dried over $MgSO_4$, filtered and the solvent was removed *in vacuo* to give the crude 1,3-dione. The dione was dissolved in ethanol (20 mL) and $N_2H_4.H_2O$ (4 mL) was added. The solution was heated to reflux overnight before being cooled to RT. The solvent was removed *in vacuo* and the residue was purified by column chromatography (hexane:EtOAc 3:2 v/v) to give an off-white solid, 2-(3-(trifluoromethyl)-1*H*-pyrazol-5-yl)pyridine **16** (1.31 g, 75%); δ_H (400 MHz; $CDCl_3$) 11.74 (1H, s), 8.65 (1H, ddd, *J* 4.9, 1.8, 1.0), 7.82 (1H, td, *J* 7.8, 1.7), 7.65 (1H, dt, *J* 7.9, 1.1), 7.33 (1H, ddd, *J* 7.6, 4.9, 1.1), 6.96 (1H, s); δ_F (376 MHz; $CDCl_3$) -62.35 (s).

Iridium complex 14

2-(2-fluoro-4-methoxy-3-tosylphenyl)-4-mesitylpyridine **10**[29] (110 mg, 0.23 mmol) and $IrCl_3.3H_2O$ (37 mg, 0.10 mmol) were combined in 2-ethoxyethanol (5 mL), and the mixture was heated to reflux overnight under a nitrogen atomsphere. The reaction was the cooled to RT, and the solvent removed *in vacuo*. The residue was redissolved in DCM/EtOH (3:1 v/v, 20 mL) and 2-(3-(trifluoromethyl)-1*H*-pyrazol-5-yl)pyridine **16** (28 mg, 0.13 mmol) and Na_2CO_3 (11 mg, 0.10 mmol) were added. The solution was heated to 55 °C for 6 h, before being cooled to RT and the solvent removed *in vacuo*. The residue was purified by column chromatography (0-3% EtOAc in DCM) to give the product as a yellow solid, iridium complex **14** (109 mg, 77%); Anal. Calc. for $C_{65}H_{55}F_5IrN_5O_6S_2$: C, 57.68; H, 4.10; N, 5.17. Found: C, 57.84; H, 4.33; N, 4.92; δ_H (400 MHz, $CDCl_3$) 8.11 (1H, s), 8.05 (1H, s), 7.95 – 7.78 (6H, m), 7.70 – 7.64 (1H, m), 7.56 (1H, d, *J* 6.0), 7.50 – 7.43 (2H, m), 7.29 (1H, d, *J* 0.8), 7.26 – 7.22 (2H, m), 7.18 – 7.11 (1H, m), 7.01 (1H, s), 6.93 (4H, d, *J* 6.4), 6.77 (1H, dd, *J* 5.9, 1.8), 6.71 (1H, dd, *J* 6.0, 1.8), 5.72 (1H, s), 5.70 (1H, s), 3.44 (3H, s), 3.41 (3H, s), 2.39 (3H, s), 2.38 (3H, s), 2.33 (6H, s), 1.99 (3H, s), 1.97 (6H, s), 1.93 (3H, s); δ_F (376 MHz; $CDCl_3$) -59.85 (3F, s), -110.73 (1F, s); -111.48 (1F, s); HRMS (FTMS+ESI): calcd for $[C_{65}H_{55}N_5O_6F_5S_2{}^{191}Ir+H]^+$: 1352.3198. Found: 1352.3193.

Iridium complex 15

2-(2,4-dimethoxy-3-(methylsulfonyl)phenyl)-4-mesitylpyridine **11**[29] (198 mg, 0.48 mmol) and $[Ir(COD)Cl]_2$ (79 mg, 0.12 mmol) were combined in 2-ethoxyethanol (5 mL), and the mixture was heated to reflux overnight under a nitrogen atmosphere. The reaction was the cooled to RT, and the solvent removed *in vacuo*. The residue was redissolved in DCM/EtOH (3:1 v/v, 20 mL) and 2-(3-(trifluoromethyl)-1*H*-pyrazol-5-yl)pyridine **16** (63 mg, 0.30 mmol) and Na_2CO_3 (50 mg, 0.47 mmol) were added. The solution was heated to 55 °C for 5 h, before being cooled to RT and the solvent removed *in vacuo*. The residue was purified by column chromatography (0-10% EtOAc in DCM) to give the product as a yellow solid, iridium complex **15** (28 mg, 56%); Anal. Calc. for $C_{55}H_{53}F_3IrN_5O_8S_2$: C, 53.91; H, 4.36; N, 5.72. Found: C, 53.48; H, 4.43; N, 5.55; δ_H (400 MHz, $CDCl_3$) 8.46 (1H, d, *J* 1.8), 8.40 (1H, d, *J* 1.8), 7.88 (2H, m), 7.82 (1H, d, *J* 5.9), 7.75 (1H, d, *J* 5.6), 7.52 (1H, d, *J* 5.9), 7.16 (1H, td, *J* 6.0, 2.6), 7.04 (1H, s), 6.98 (2H, s), 6.96 (2H, s), 6.85 (1H, dd, *J* 5.9, 1.9), 6.72 (1H, dd, *J* 5.9, 1.9), 5.96 (1H, s), 5.89 (1H, s), 3.91 (3H, s), 3.91 (3H, s), 3.60 (3H, s), 3.58 (3H, s), 3.30 (3H, s), 3.27 (3H, s), 2.35 (6H, s), 2.03 (6H, s), 2.01 (3H, s), 1.97 (3H, s); δ_F (376 MHz; $CDCl_3$) -60.00 (s); HRMS (FTMS+ESI): calcd for $[C_{55}H_{53}N_5O_8F_3S_2{}^{191}Ir+H]^+$: 1224.2972. Found: 1224.2987.

Acknowledgements

We thank EPSRC grant EL/L02621X/1 for funding the work in Durham.

References

[1] V. W.-W. Yam, K. M.-C. Wong, *Chem. Comm.,* 2011, **47**, 11579.
[2] M. A. Baldo, D. F. O'Brien, Y. You, A. Shoustikov, S. Sibley, M. E. Thompson, S. R. Forrest, *Nature*, 1998, **395**, 151.
[3] H. Yersin, *Highly Efficient OLEDs with Phosphorescent Materials*; Wiley-VCH: Darmstadt, 2008.
[4] M. S. Lowry, S. Bernhard, *Chem. Eur. J.*, 2006, **12**, 7970.
[5] K. K.-W. Lo, W.-K. Hui, C.-K. Chung, K. H.-K. Tsang, D. C.-M. Ng, N. Zhu, K.-K. Cheung, *Coord. Chem. Rev.*, 2005, **249**, 1434.

[6] K. Müllen, U. Scherf, *Organic Light Emitting Devices: Synthesis, Properties and Applications*; Wiley-VCH Verlag GmbH & Co. KGaA, 2006.
[7] R. Mertens, The OLED Handbook. A Guide to OLED Technology, Industry and Market, 2014: www.oled-info.com/handbook.
[8] Z.-R. Li, H. Meng, *Organic Light-Emitting Materials and Devices*; CRC Press: Boca Raton, Florida, 2006.
[9] M. Du, Y. Feng, D. Zhu, T. Peng, Y. Liu, Y. Wang, M.R. Bryce, *Adv. Mater.*, 2016, **28**, 5963.
[10] L. Ying, C.-L. Ho, H. Wu, Y. Cao, W.-Y. Wong, *Adv. Mater.*, 2014, **26**, 2459.
[11] E. Holder, B. M. W. Langeveld, U. S. Schubert, *Adv. Mater.*, 2005, **17**, 1109.
[12] P. T. Chou, Y. Chi, *Chem. Eur. J.*, 2007, **13**, 380.
[13] X. Yang, G. Zhou, W.-Y. Wong, *Chem. Soc. Rev.*, 2015, **44**, 8484.
[14] Y. You, S. Y. Park, *Dalton Trans.*, 2009, 1267.
[15] S. Ladouceur, E. Zysman-Colman, *Eur. J. Inorg. Chem.*, **2013**, 2985.
[16] E. Baranoff, B.F. Curchod, *Dalton Trans.*, 2015, **44**, 8318.
[17] S. H. Kim, J. Jang, S. J Lee, J. Y. Lee, *Thin Solid Films*, 2008, **517**, 722.
[18] S. Lamansky, P. Djurovich, D. Murphy, F. Abdel-Razzaq, R. Kwong, I. Tsyba, M. Bortz, B. Mui, R. Bau, M. E. Thompson, *Inorg. Chem.*, 2001, **40**, 1704.
[19] T. Sajoto, P. I. Djurovich, A. Tamayo, M. Yousufuddin, R. Bau, M. E. Thompson, R. J. Holmes, S. R. Forrest, *Inorg. Chem.,* 2005, **44**, 7992.
[20] C. Fan, Y. Li, C. Yang, H. Wu, J. Qin, Y. Cao, *Chem. Mater.*, 2012, **24**, 4581.
[21] J. B. Kim, S. H. Han, K. Yang, S. K. Kwon, J. J. Kim, Y. H. Kim, *Chem. Commun.*, 2015, **51**, 58.
[22] S. Lee, S. O. Kim, H. Shin, H. J. Yun, K. Yang, S. K. Kwon, J. J. Kim, Y. H. Kim, *J. Am. Chem. Soc.*, 2013, **135**, 14321.
[23] L.-L. Wu, C.-H. Yang, I.W. Sun, S.-Y. Chu, P.-C. Kao, H.-H. Huang, *Organometallics*, 2007, **26**, 2017.
[24] H. Oh, K.-M. Park, H. Hwang, S. Oh, J. H. Lee, J.-S. Lu, S. Wang, Y. Kang, *Organometallics*, 2013, **32**, 6427.
[25] E. Orselli, G. S. Kottas, A. E. Konradsson, P. Coppo, R. Frohlich, L. de Cola, A. van Dijken, M. Buchel, H. Borner, *Inorg. Chem.*, 2007, **46**, 11082.
[26] J. Li, P. I. Djurovich, B. D. Alleyne, M. Yousufuddin, N. N. Ho, J. C. Thomas, J. C. Peters, R. Bau, M. E. Thompson, *Inorg. Chem.*, 2005, **44**, 1713.
[27] J. Li, P. I. Djurovich, B. D. Alleyne, I. Tsyba, N. N. Ho, R. Bau, M. E. Thompson, *Polyhedron*, 2004, **23**, 419.
[28] H.-J. Seo, K.-M. Yoo, M. Song, J. S. Park, S.-H. Jin, Y. I. Kim, J.-J. Kim, *Org. Electron.*, 2010, **11**, 564.
[29] H. Benjamin, Y. Zheng, A. S. Batsanov, M. A. Fox, H. A. Al-Attar, A. P. Monkman, M. R. Bryce, *Inorg. Chem.*, 2016, **55**, 8612.
[30] C.-H. Yang, M. Mauro, F. Polo, S. Watanabe, I. Muenster, R. Fröhlich, L. De Cola, *Chem. Mater.*, 2012, **24**, 3684.
[31] C. H. Hsieh, F. I. Wu, C. H. Fan, M. J. Huang, K. Y. Lu, P. Y. Chou, Y. H. Yang, S. H. Wu, I. C. Chen, S. H. Chou, K. T. Wong, C. H. Cheng, *Chem. Eur. J.*, 2011, **17**, 9180.
[32] H. Fu, Y.-M. Cheng, P.-T. Chou, Y. Chi, *Mater. Today*, 2011, **14**, 472.
[33] L. Shi, B. Hong, W. Guan, Z. Wu, Z. Su, *J. Phys. Chem. A*, 2010, **114**, 6559.
[34] J. M. Fernandez-Hernandez, J. I. Beltran, V. Lemaur, M. D. Galvez-Lopez, C. H. Chien, F. Polo, E. Orselli, R. Frohlich, J. Cornil, L. De Cola, *Inorg. Chem.*, 2013, **52**, 1812.
[35] C.-H. Chang, C.-C. Chen, C.-C. Wu, C.-H. Yang, Y. Chi, *Org. Electron.*, 2009, **10**, 1364.
[36] J. Frey, B. F. E. Curchod, R. Scopelliti, I. Tavernelli, U. Rothlisberger, M. K. Nazerruddin, E. Baranoff, *Dalton Trans*. 2014, **43**, 5667.
[37] V. N. Kozhevnikov, K. Dahms, M. R. Bryce, *J. Org. Chem*., 2011, **76**, 5143.
[38] S. Schmidbauer, A. Hohenleutner, B. Konig, *Adv. Mater.* **2013**, *25*, 2114.
[39] V. N. Kozhevnikov, Y. Zheng, M. Clough, H. A. Al-Attar, G. C. Griffiths, K. Abdullah, S. Raisys, V. Jankus, M. R. Bryce, A. P. Monkman, *Chem. Mater.*, 2013, **25**, 2352.
[40] A. F. Henwood, A. K. Bansal, D. B. Cordes, A. M. Z. Slawin, I. D. W. Samuel, E. Zysman-Colman, *J. Mater. Chem. C,* **2016**, *4*, 3726.
[41] (a) D. Rota Martir, A. K. Bansal, V. Di Mascio, D. B. Cordes, A. F. Henwood, A. M. Z. Slawin, P. C. J. Kamer, L. Martinez-Sarti, A. Pertegas, H. J. Bolink, I. D. W. Samuel, E. Zysman-Colman, *Inorg. Chem. Front.*, 2016, **3**, 218. (b) D. Rota Martir, G. J. Hedley, D. B. Cordes, A. M. Z. Slawin, D. Escudero, D. Jacquemin, T. Kosikova, D. Philip, D. M. Dawson, S. E. Ashbrook, I. D. W. Samuel, E. Zysman-Colman, *Dalton Trans*., 2016, **45**, 17195. (c) D. Rota Martir, C. Momblona, A. Pertegás, D. B. Cordes, A. M. Z. Slawin, H. J. Bolink, E. Zysman-Colman, *ACS Appl. Mater. Interfaces*, 2016, **8**, 33907.
[42] J. Li, Q. Zhang, H. He, L. Wang, J. Zhang, *Dalton Trans.*, 2015, **44**, 8577.
[43] E. Bisagni, M. Rautureau, C. Huel, *Heterocycles*, 1989, **29**, 1815.
[44] E. Busto, V. Gotor-Fernández, V. Gotor, *Tetrahedron: Asymmetry*, 2006, **17**, 1007.
[45] C.-C. Cheng, W.-S. Yu, P.-T. Chou, S.-M. Peng, G.-H. Lee, P.-C. Wu, Y.-H. Song, Y. Chi, *Chem. Comm.,* 2003, 2628.
[46] C.-H. Lin, Y.-C. Chiu, Y. Chi, Y.-T. Tao, L.-S. Liao, M.-R. Tseng, G.-H. Lee, *Organometallics*, 2012, **31**, 4349.
[47] M. Nonoyama, *Bull. Chem. Soc. Jpn.*, 1974, **47**, 767.
[48] C. Adachi, R. C. Kwong, P. Djurovich, V. Adamovich, M. A. Baldo, M. E. Thompson, S. R. Forrest, *Appl. Phys. Lett.*, 2001, **79**, 2082.
[49] P. J. Hay, *J. Phys. Chem. A*, 2002, **106**, 1634.
[50] N. G. Connelly, W. E. Geiger, *Chem. Rev*., 1996, **96**, 877.
[51] D. Tordera, J. J. Serrano-Pérez, A. Pertegás, E. Ortí, H. J. Bolink, E. Baranoff, M. K. Nazeeruddin, J. Frey, *Chem. Mater.*, 2013, **25**, 3391.
[52] V. Sivasubramaniam, F. Brodkorb, S. Hanning, H. P. Loebl, V. van Elsbergen, H. Boerner, U. Scherf, M. Kreyenschmidt, *J. Fluorine Chem.*, 2009, **130**, 640.
[53] V. Sivasubramaniam, F. Brodkorb, S. Hanning, H. Loebl, V. Elsbergen, H. Boerner, U. Scherf, M. Kreyenschmidt, *Central European Journal of Chemistry*, 2009, *7*, 836.
[54] R. Seifert, I. Rabelo de Moraes, S. Scholz, M. C. Gather, B. Lüssem, K. Leo, *Org. Electron.*, 2013, **14**, 115.
[55] J.-H. Jou, W.-B. Wang, S.-M. Shen, S. Kumar, I. M. Lai, J.-J. Shyue, S. Lengvinaite, R. Zostautiene, J. V. Grazulevicius, S. Grigalevicius, S.-Z. Chen, C.-C. Wu, *J. Mater. Chem.*, 2011, **21**, 9546.
[56] S.-J. Su, Y. Takahashi, T. Chiba, T. Takeda, J. Kido, *Adv. Funct. Mater.*, 2009, **19**, 1260.
[57] D. Sun, H. Zhou, H. Li, X. Sun, Y. Zheng, Z. Ren, D. Ma, M. R. Bryce, S. Yan, *J. Mater. Chem. C*, 2014, **2**, 8277.
[58] Gaussian 09, Revision A.02, M. J. Frisch, G. W. Trucks, H. B. Schlegel, G. E. Scuseria, M. A. Robb, J. R. Cheeseman, G. Scalmani, V. Barone, B. Mennucci, G. A. Petersson, H. Nakatsuji, M. Caricato, X. Li, H. P. Hratchian, A. F. Izmaylov, J. Bloino, G. Zheng, J. L. Sonnenberg, M. Hada, M. Ehara, K. Toyota, R. Fukuda, J. Hasegawa, M. Ishida, T. Nakajima, Y. Honda, O. Kitao, H. Nakai, T. Vreven, J. A. Montgomery, Jr., J. E. Peralta, F. Ogliaro, M. Bearpark, J. J. Heyd, E. Brothers, K. N. Kudin, V. N. Staroverov, R. Kobayashi, J. Normand, K. Raghavachari, A. Rendell, J. C. Burant, S. S. Iyengar, J. Tomasi, M. Cossi, N. Rega, J. M. Millam, M. Klene, J. E. Knox, J. B. Cross, V.

Bakken, C. Adamo, J. Jaramillo, R. Gomperts, R. E. Stratmann, O. Yazyev, A. J. Austin, R. Cammi, C. Pomelli, J. W. Ochterski, R. L. Martin, K. Morokuma, V. G. Zakrzewski, G. A. Voth, P. Salvador, J. J. Dannenberg, S. Dapprich, A. D. Daniels, O. Farkas, J. B. Foresman, J. V. Ortiz, J. Cioslowski, D. J. Fox, *Gaussian, Inc.*, Wallingford CT, 2009.

[59] (a) A. D. Becke, *J. Chem. Phys.,* 1993, **98**, 5648. (b) C. Lee, W. Yang, R. G. Parr, *Phys. Rev. B*, 1988, **37**, 785.

[60] (a) T. H. Dunning, Jr.; P. J. Hay, *Modern Theoretical Chemistry*, Ed. H. F. Schaefer III, Vol. 3 Plenum, New York, 1976. (b) P. J. Hay, W. R. Wadt, *J. Chem. Phys.*, 1985, **82**, 270. (c) W. R. Wadt, P. J. Hay, *J. Chem. Phys.*, 1985, **82**, 284. (d) P. J. Hay, W. R. Wadt, *J. Chem. Phys.*, 1985, **82**, 299.

[61] (a) G. A. Petersson, M. A. Al-Laham, *J. Chem. Phys.*, 1991, **94**, 6081. (b) G. A. Petersson, A. Bennett, T. G. Tensfeldt, M. A. Al-Laham, W. A. Shirley, J. Mantzaris, *J. Chem. Phys.*, 1988, **89**, 2193.

[62] A. R. Allouche, *J. Comput. Chem*., 2011, **32**, 174.

[63] N. M. O'Boyle, A. L. Tenderholt, K. M. Langner, *J. Comput. Chem*., 2008, **29**, 839.

[64] G. Sheldrick, *Acta Crystallogr. A*, 2008, **64**, 112.

[65] G. Sheldrick, *Acta Crystallogr. C*, 2015, **71**, 3.

[66] L. J. Bourhis, O. V. Dolomanov, R. J. Gildea, J. A. K. Howard, H. Puschmann, *Acta Crystallogr. A*, 2015, **71**, 59.

[67] A. Spek, *Acta Crystallogr. D*, 2009, **65**, 148.

[68] P. van der Sluis, A. L. Spek, *Acta Crystallogr. A*, 1990, **46**, 194.

Supporting Information

Pyridylpyrazole N^N Ligands Combined with Sulfonyl-Functionalized Cyclometalating Ligands for Blue-Emitting Iridium(III) Complexes and Solution-Processable PhOLEDs

Helen Benjamin,[†] Mark A. Fox,[†] Andrei S. Batsanov,[†] Hameed A. Al-Attar,[‡] Chensen Li, [§] Zhongjie Ren,[§] Andrew P. Monkman,[‡] and Martin R. Bryce*,[†]

[†]*Department of Chemistry, Durham University, Durham DH1 3LE, U.K.* *m.r.bryce@durham.ac.uk*

[‡] *Department of Physics, Durham University, Durham DH1 3LE, U.K.*

[§] *State Key Laboratory of Chemical Resource Engineering, Beijing University of Chemical Technology, Beijing 100029, China*

Contents

Copies of NMR spectra

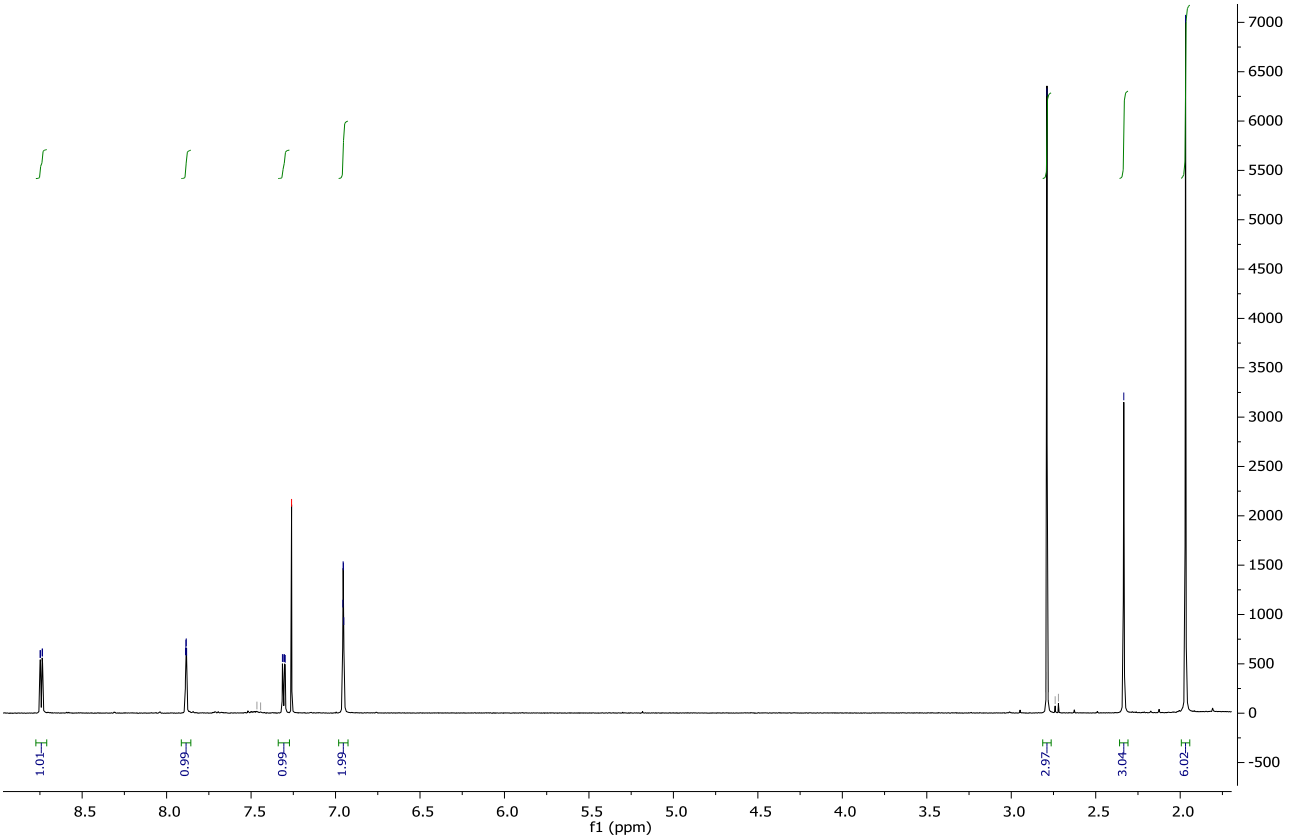

Figure S1. ^{1}H NMR spectrum of **7** in $CDCl_3$.

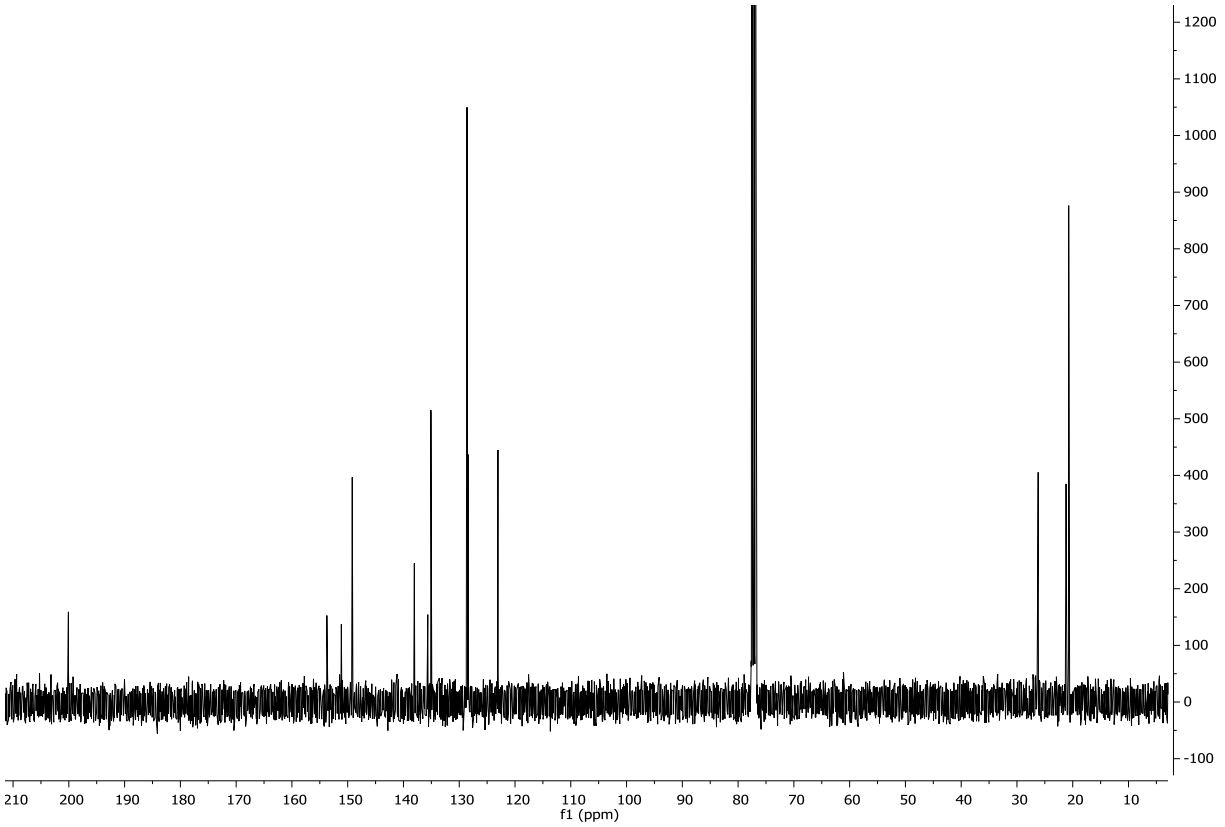

Figure S2. ^{13}C NMR spectrum of **7** in $CDCl_3$.

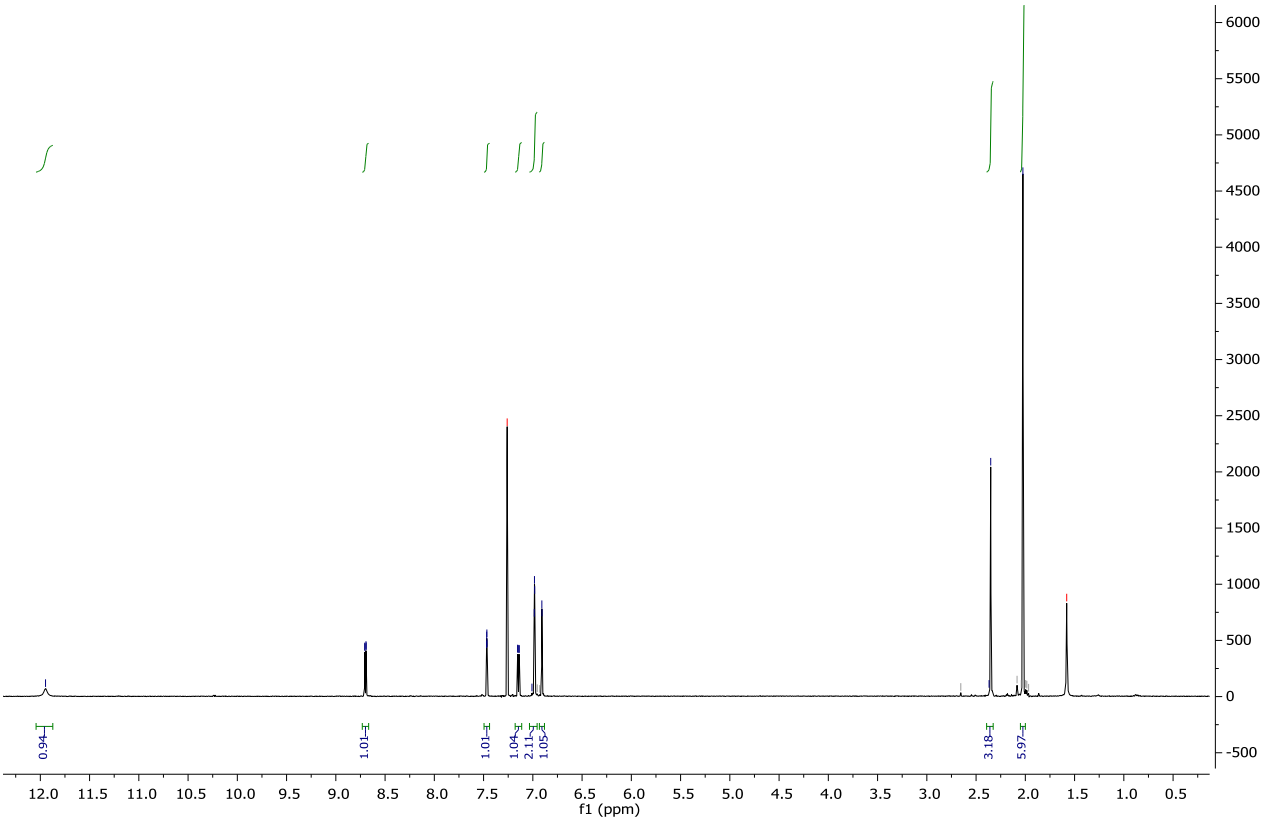

Figure S3. ^{1}H NMR spectrum of **9** in $CDCl_3$.

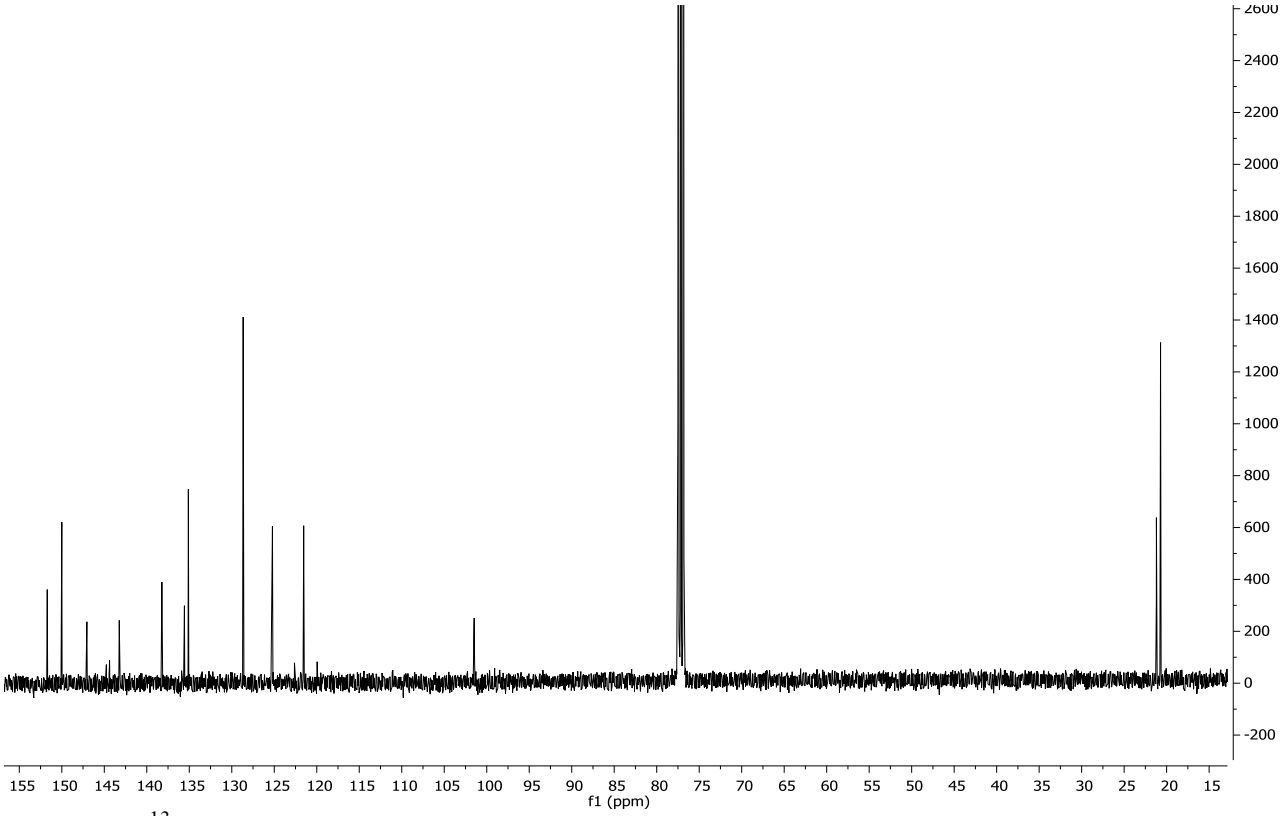

Figure S4. ^{13}C NMR spectrum of **9** in $CDCl_3$.

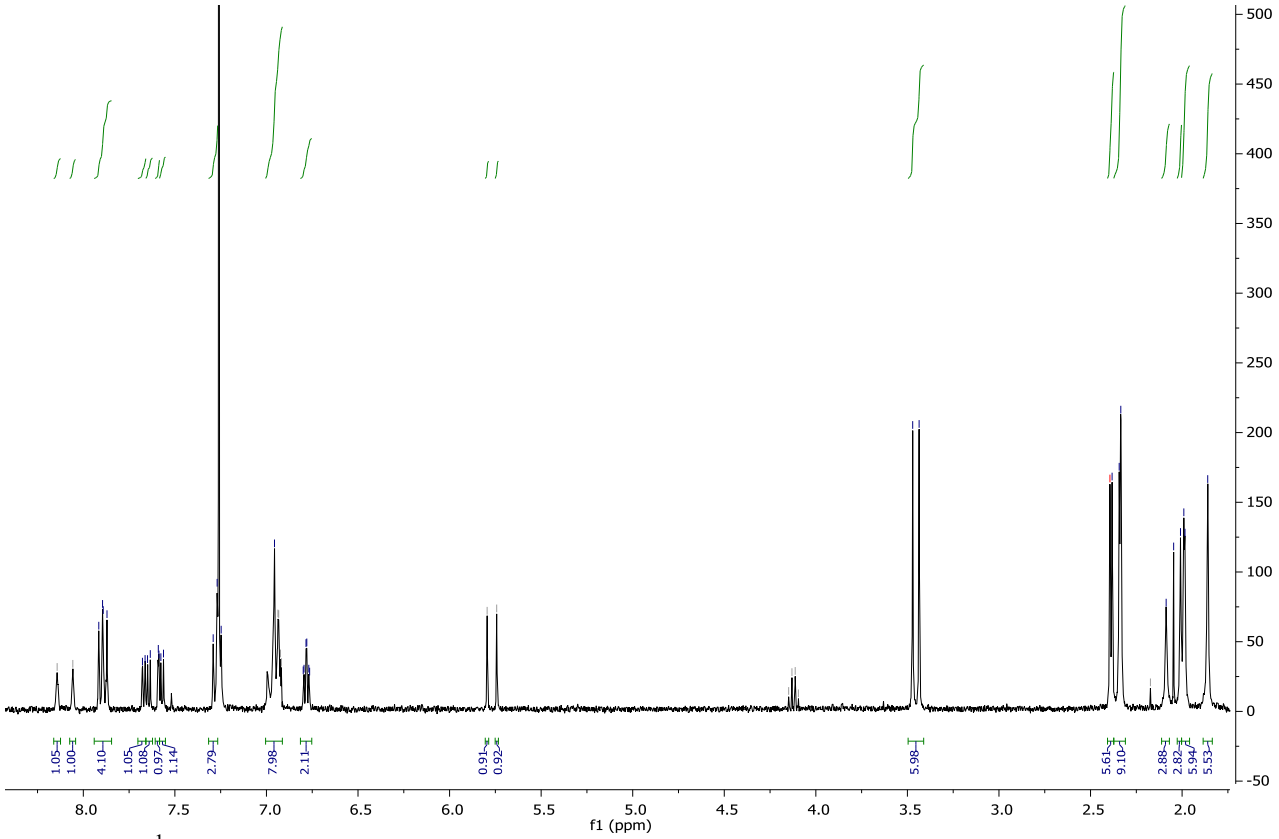

Figure S5. ^{1}H NMR spectrum of **12** in $CDCl_3$.

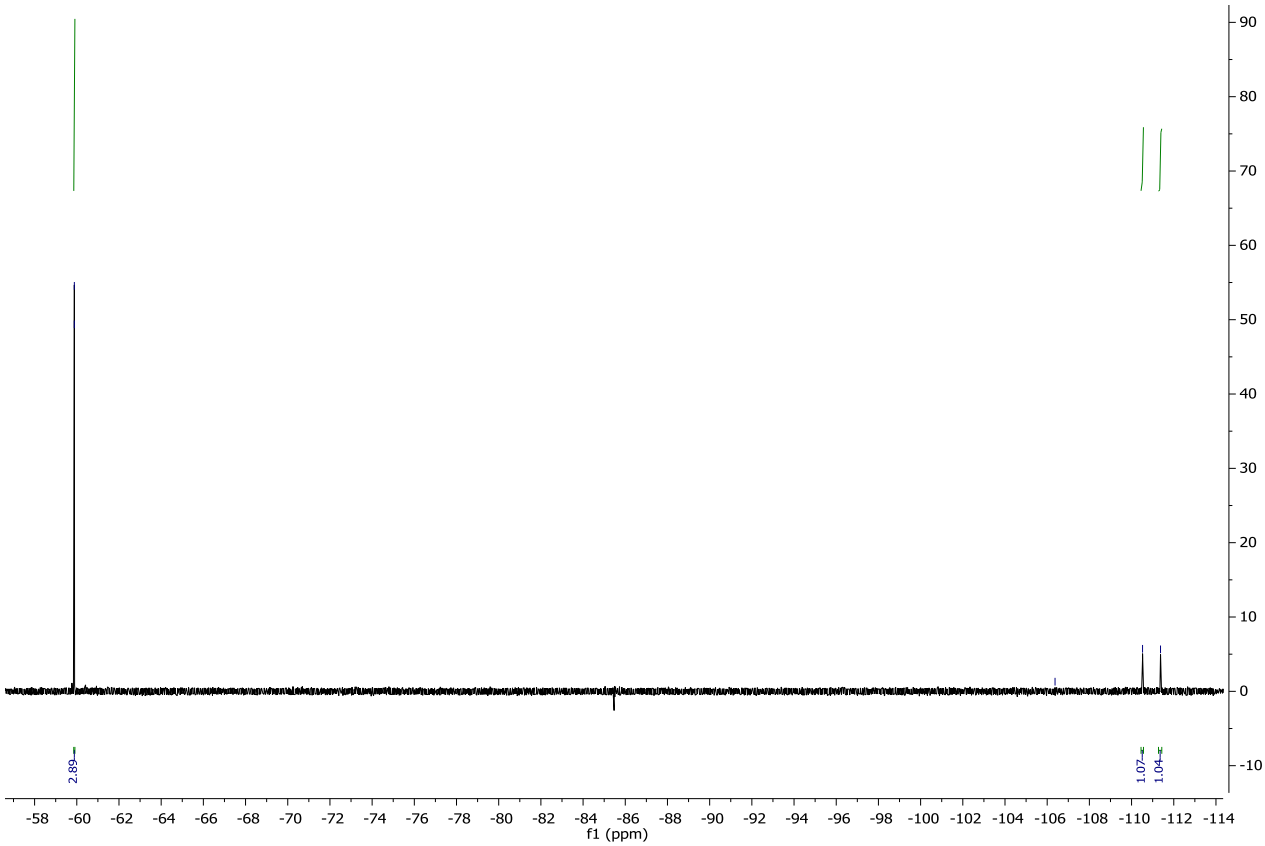

Figure S6. ^{19}F NMR spectrum of **12** in $CDCl_3$.

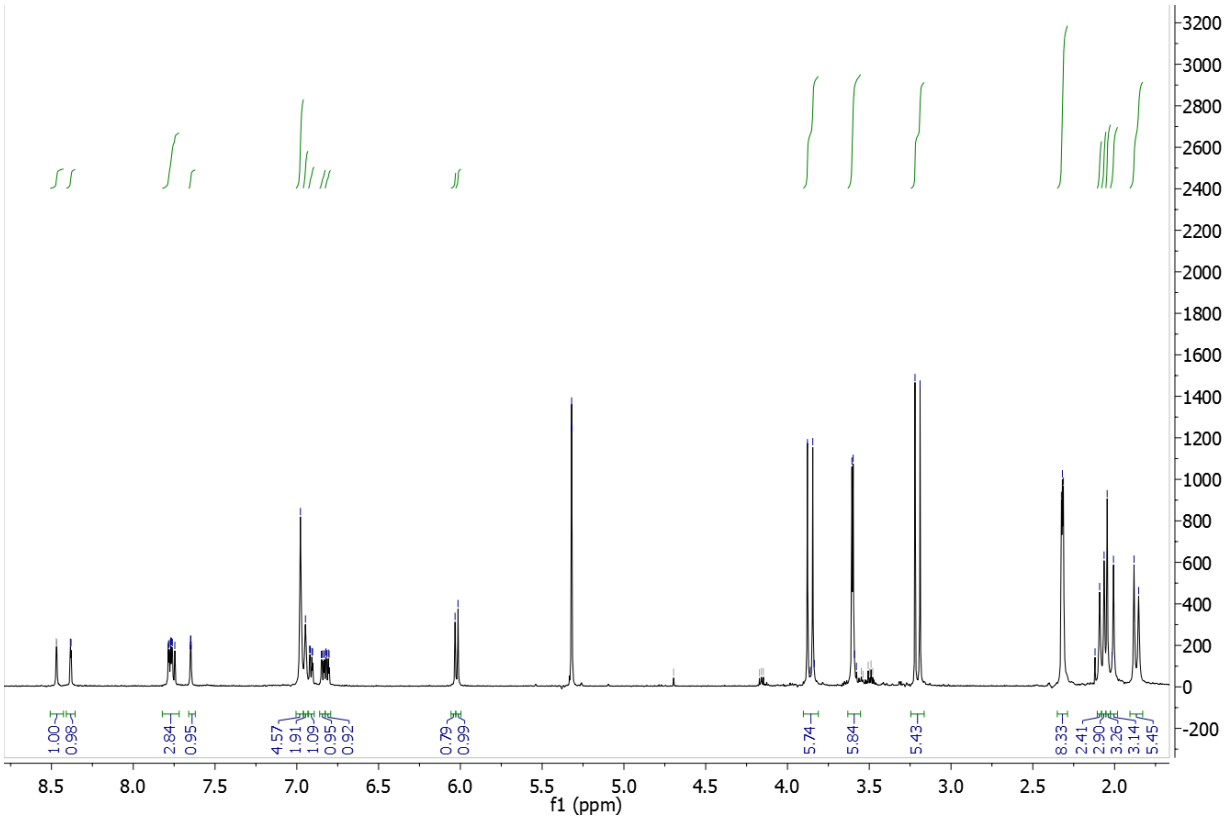

Figure S7. ^{1}H NMR spectrum of **13** in $CDCl_3$.

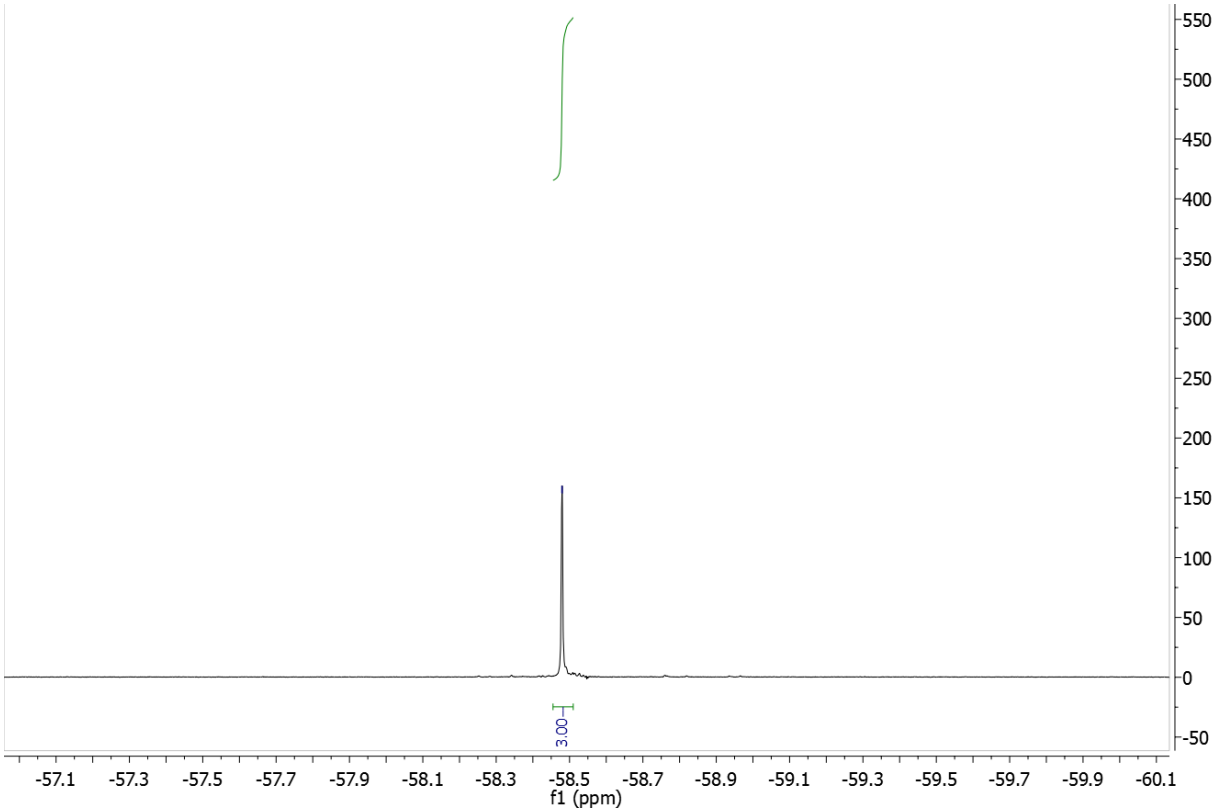

Figure S8. ^{19}F NMR spectrum of **13** in $CDCl_3$.

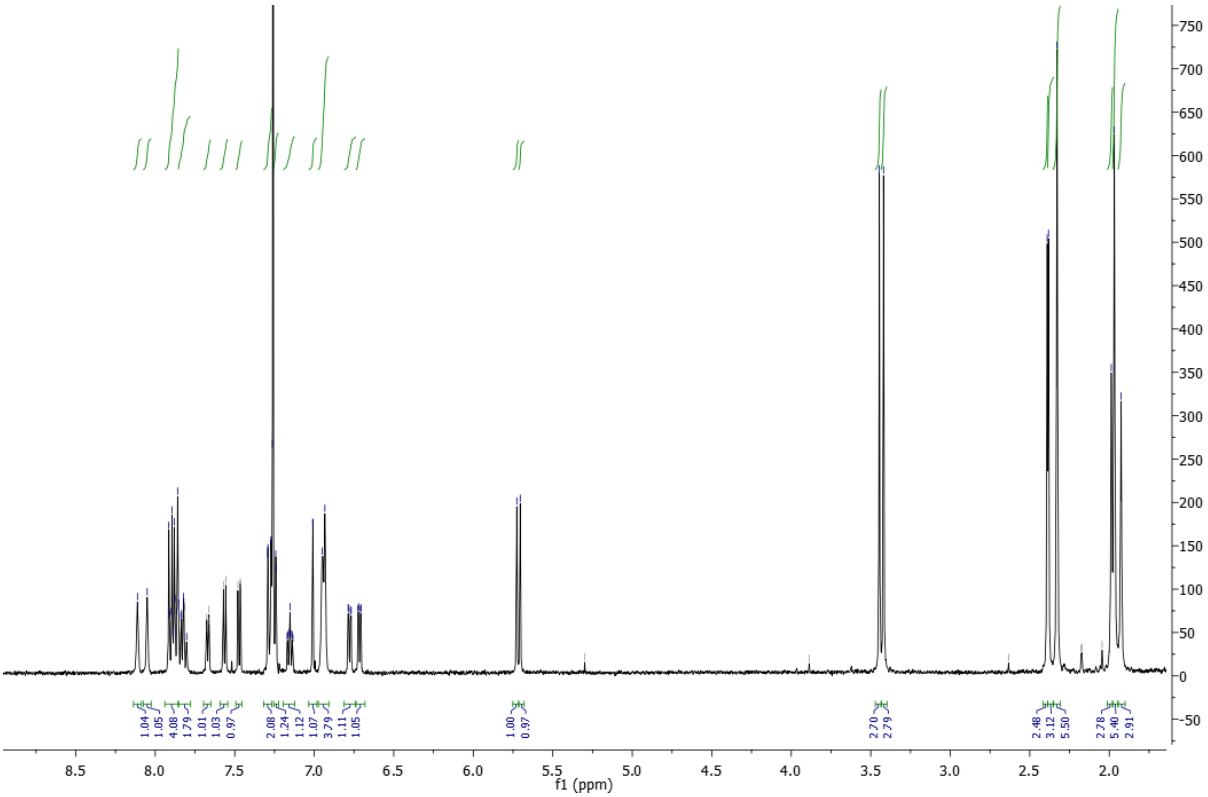

Figure S9. ^{1}H NMR spectrum of **14** in $CDCl_3$.

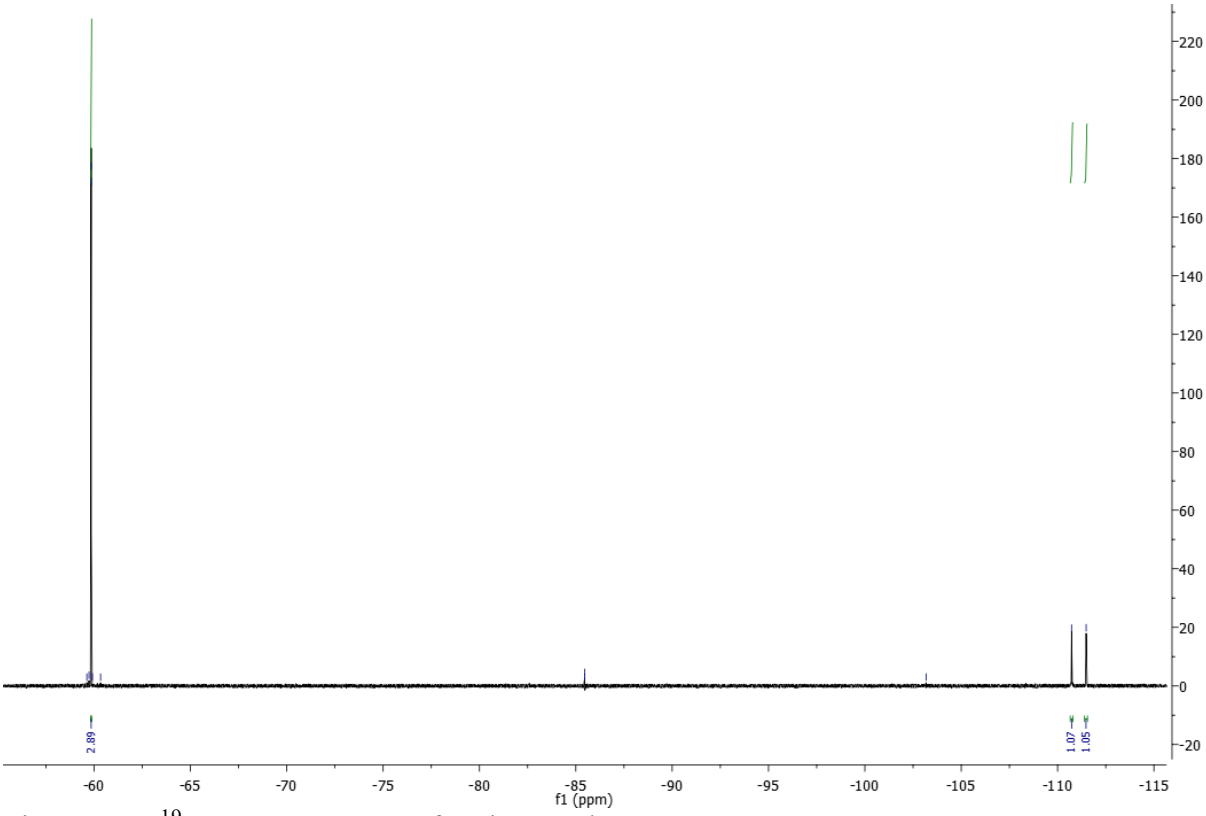

Figure S10. ^{19}F NMR spectrum of **14** in $CDCl_3$.

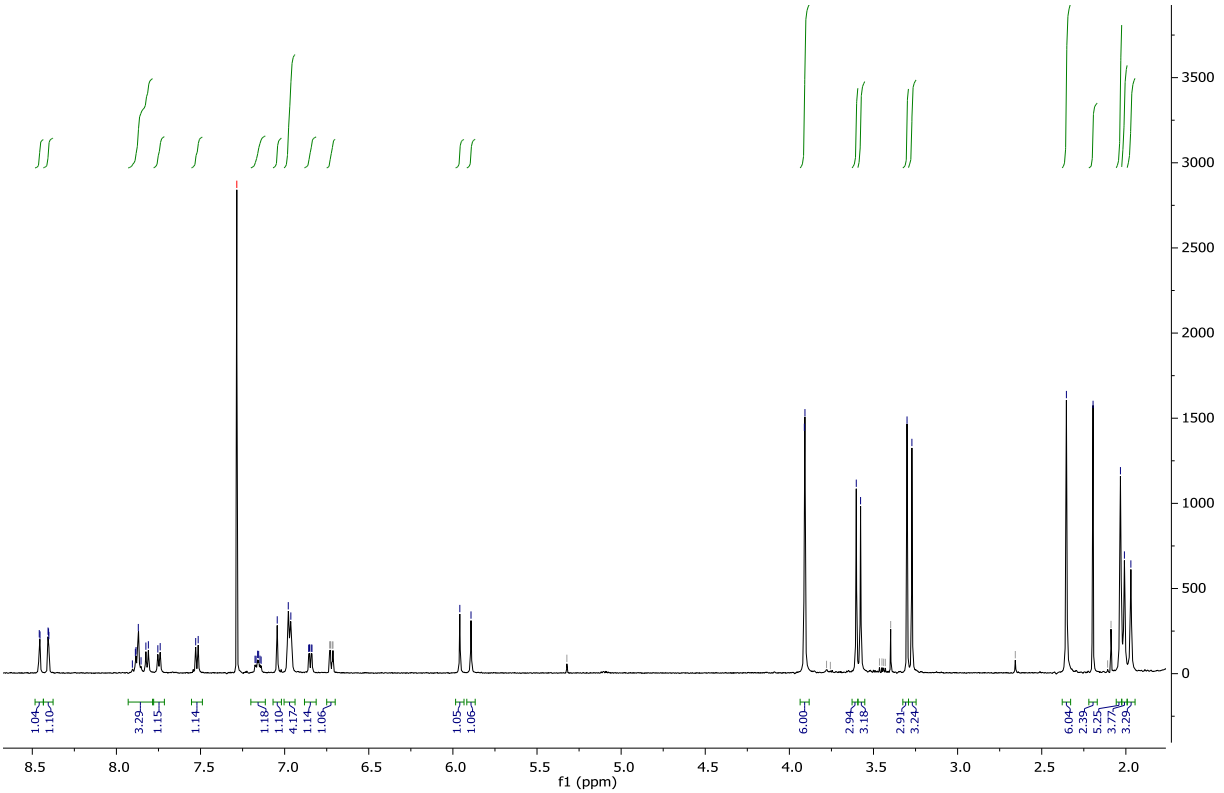

Figure S11. ^{1}H NMR spectrum of **15** in $CDCl_3$.

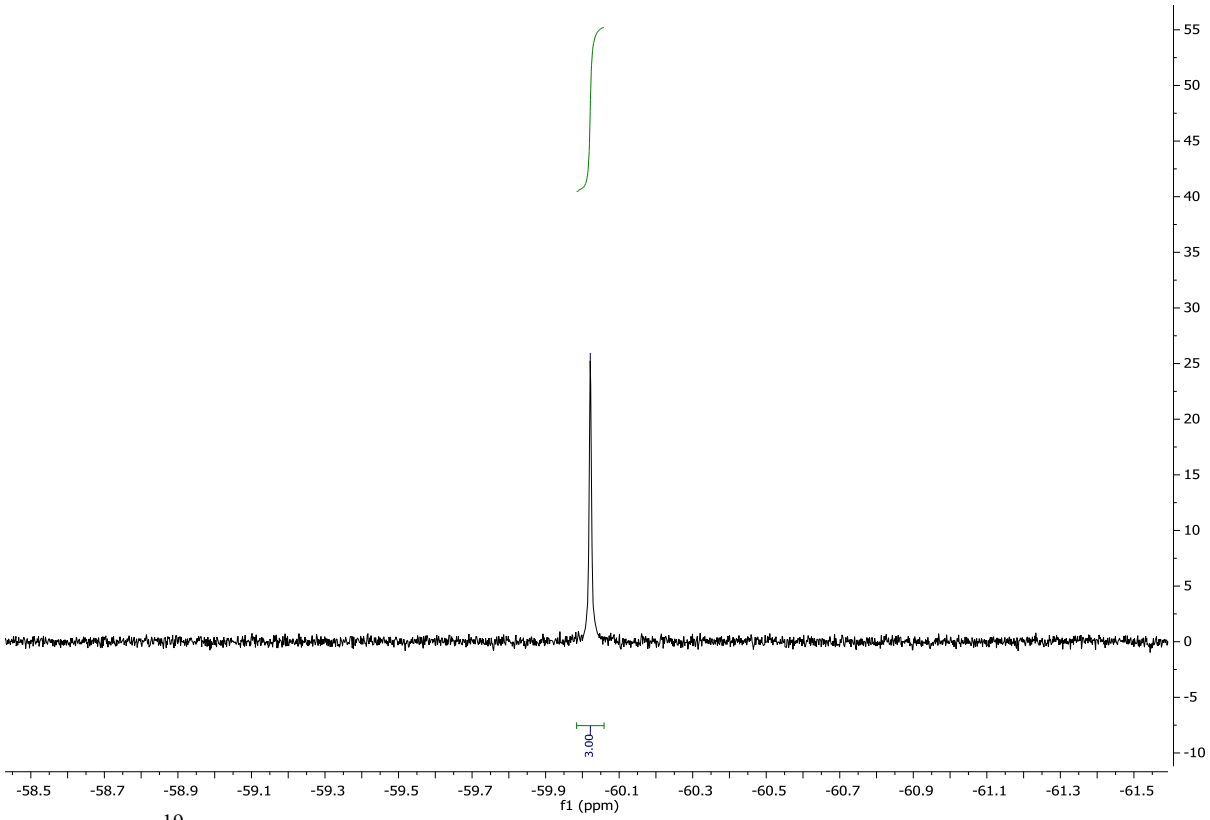

Figure S12. ^{19}F NMR spectrum of **15** in $CDCl_3$.

Table S1. MO energies and %MO contributions for important MOs in **12′**. Pz = pyrazylene, Py(pypz) = pyridylene in pypz ligand, Ph = phenylene, pyridylene in ppy ligand.

MO		eV	Pz	Py(pypz)	Ph	Ir	Py(ppy)
347	LUMO+3	-1.30	7	62	4	1	26
346	LUMO +2	-1.62	1	1	22	4	72
345	LUMO +1	-1.74	8	44	12	6	30
344	LUMO	-1.83	7	36	14	2	41
343	HOMO	-5.74	3	1	51	33	12
342	HOMO -1	-5.96	24	2	25	39	10
341	HOMO -2	-6.12	15	4	50	16	15
340	HOMO -3	-6.26	24	7	37	24	8

Table S2. MO energies and %MO contributions for important MOs in **13′**.

MO		eV	Pz	Py(pypz)	Ph	Ir	Py(ppy)
315	LUMO +3	-1.24	8	73	2	1	16
314	LUMO +2	-1.51	1	4	22	4	69
313	LUMO +1	-1.65	3	22	19	6	50
312	LUMO	-1.77	12	56	8	2	22
311	HOMO	-5.62	3	0	51	33	13
310	HOMO -1	-5.86	19	1	31	39	10
309	HOMO -2	-6.01	16	3	46	20	15
308	HOMO -3	-6.15	8	3	54	25	10

Table S3. MO energies and %MO contributions for important MOs in **14′**.

MO		eV	Pz	Py(pypz)	Ph	Ir	Py(ppy)
315	LUMO +3	-1.35	8	66	3	1	22
314	LUMO +2	-1.65	1	1	22	4	72
313	LUMO +1	-1.79	4	25	18	6	47
312	LUMO	-1.89	11	55	8	2	24
311	HOMO	-5.77	3	0	53	32	12
310	HOMO -1	-6.00	23	2	27	38	10
309	HOMO -2	-6.15	14	3	51	17	15
308	HOMO -3	-6.29	11	3	56	21	9

Table S4. MO energies and %MO contributions for important MOs in **15′**.

MO		eV	Pz	Py(pypz)	Ph	Ir	Py(ppy)
283	LUMO +3	-1.29	9	75	1	1	14
282	LUMO +2	-1.53	1	2	23	4	70
281	LUMO +1	-1.68	1	13	22	5	59
280	LUMO	-1.84	13	68	4	2	13
279	HOMO	-5.64	2	0	53	32	13
278	HOMO -1	-5.89	17	1	35	36	11
277	HOMO -2	-6.04	17	3	43	22	15
276	HOMO -3	-6.18	5	2	60	22	11

Cyclic voltammetry

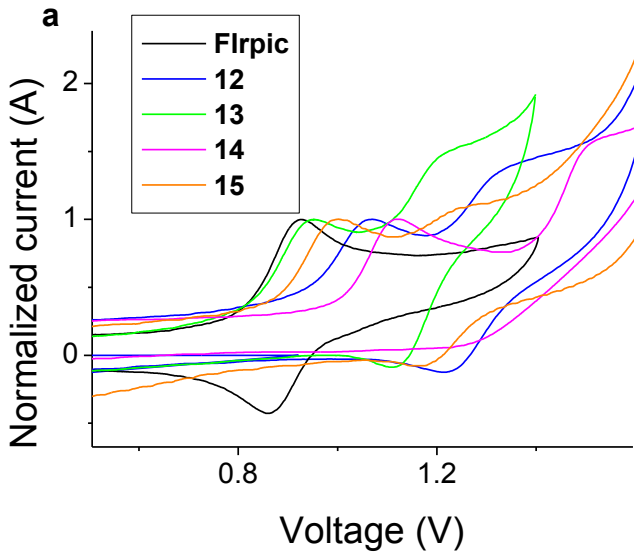

Figure S13. Cyclic voltammograms showing two oxidation waves for iridium complexes **12-15**.

Thermal properties

Table S5. Thermal stability data for all complexes using thermal gravimetric analysis (TGA) under a nitrogen atmosphere.

Complex	T_d (°C)[a]
FIrpic (1)	370
1	387
2	367
12	351
13	306
14	300
15	316

[a] Defined as the 5% weight loss temperature.

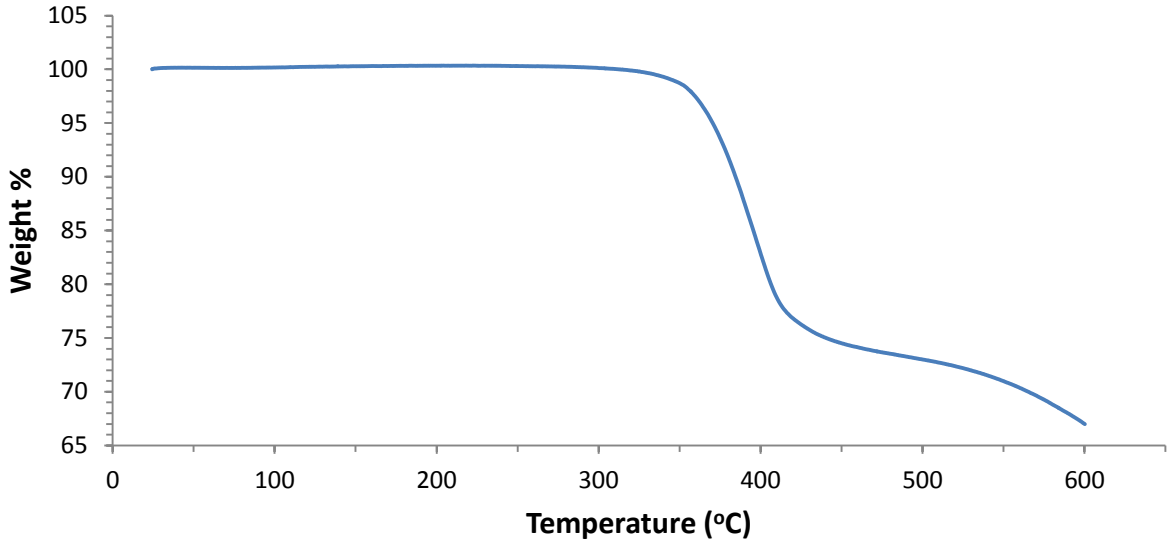

Figure S14. TGA curve for FIrpic.

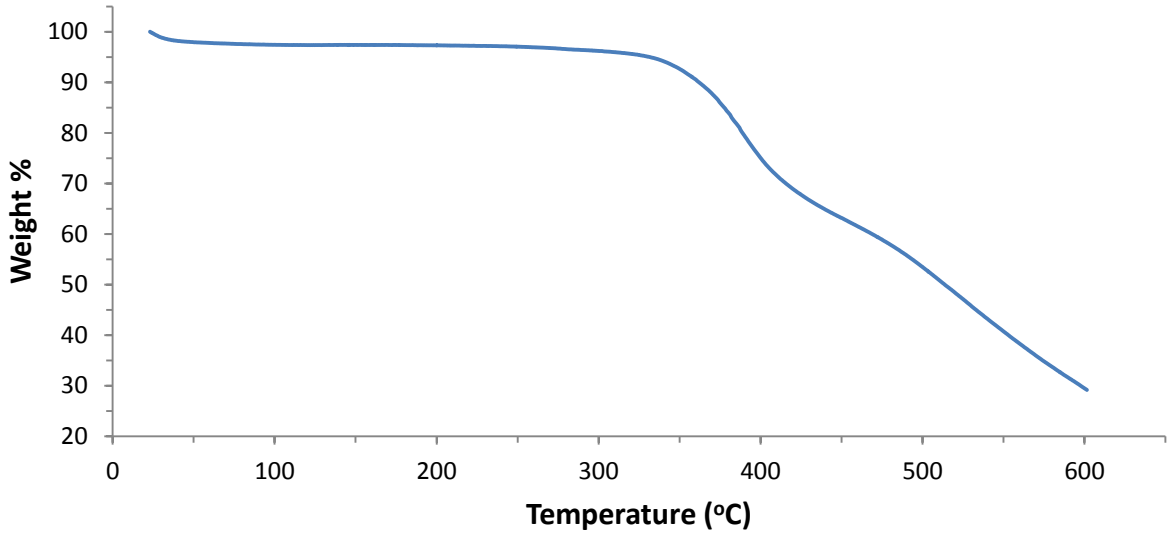

Figure S15. TGA curve for **12**. The T_d is determined after the initial solvent loss.

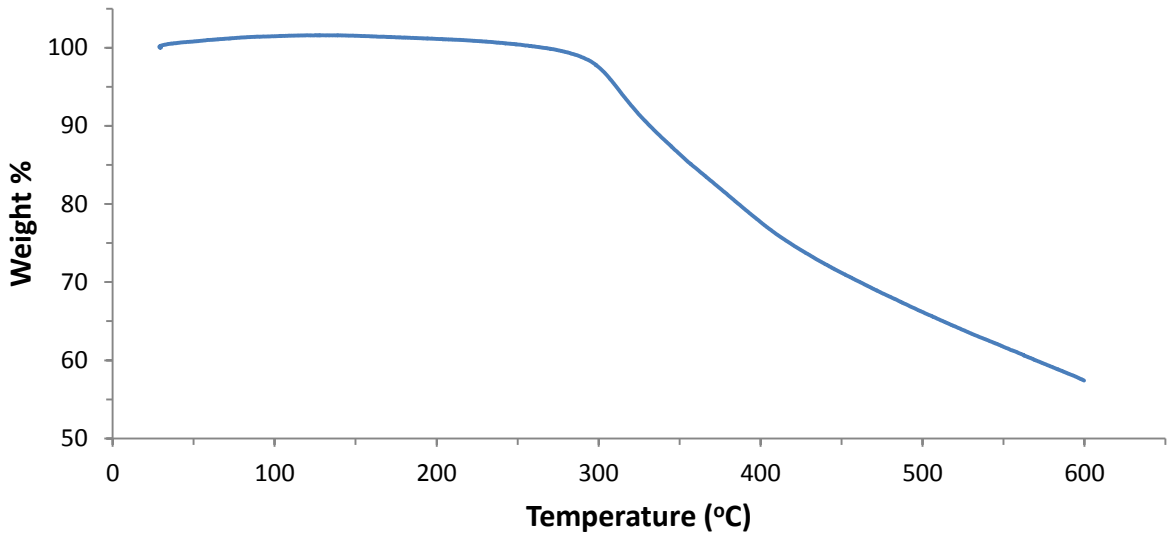

Figure S16. TGA curve for **13**.

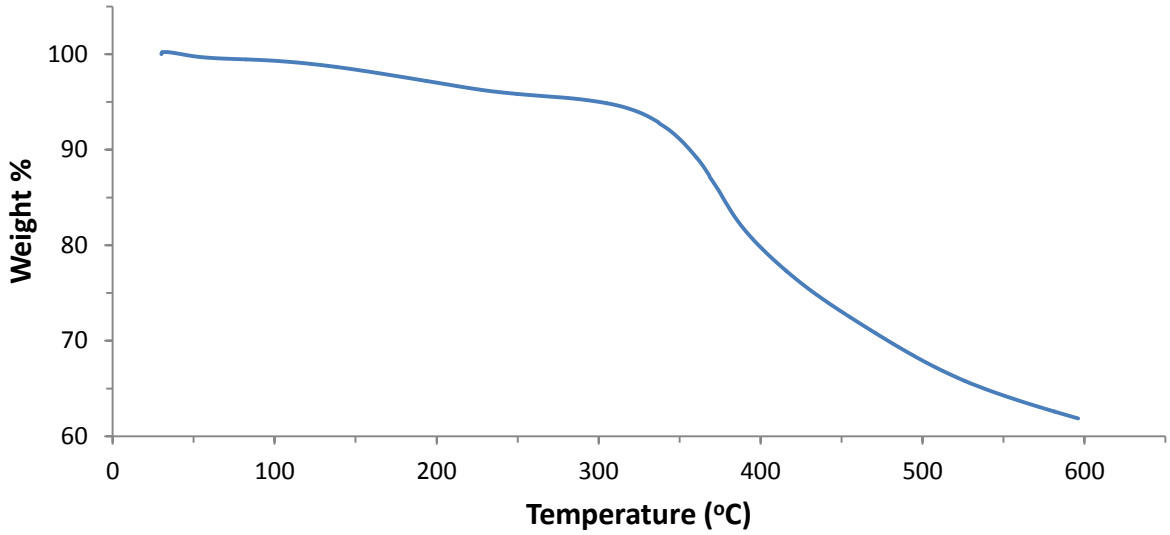

Figure S17. TGA curve for **14**.

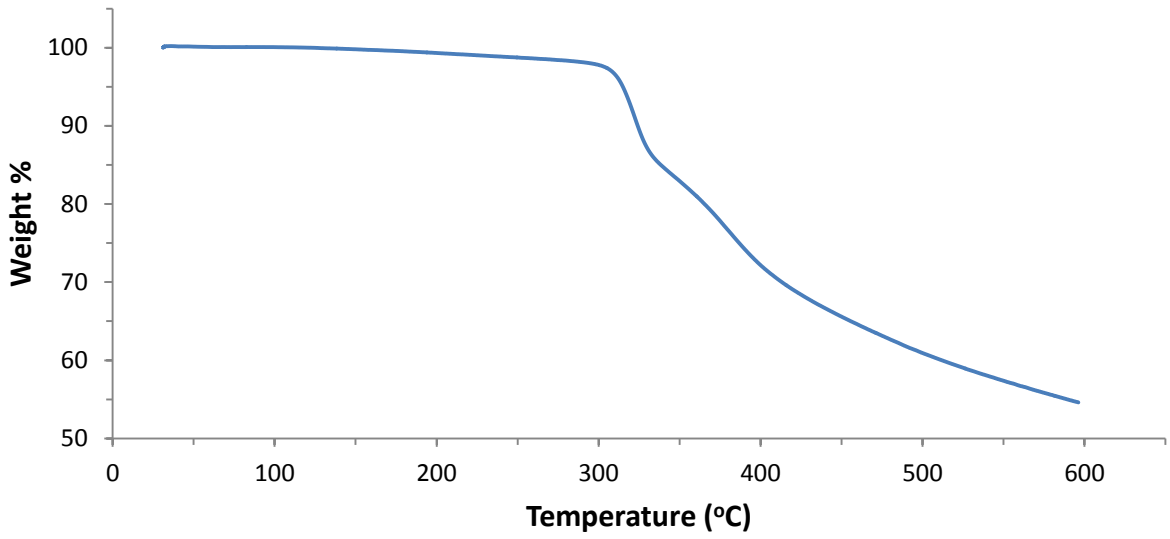

Figure S18. TGA curve for **15**.